Chem Soc Rev

Icosahedral Boron Clusters: a perfect tool for the enhancement of polymer features

Journal:	*Chemical Society Reviews*
Manuscript ID	CS-TRV-02-2016-000159.R1
Article Type:	Tutorial Review
Date Submitted by the Author:	23-Apr-2016
Complete List of Authors:	Nunez, Rosario; Consejo Superior de Investigaciones Cientificas, Instituto de Ciencia de Materiales de Barcelona Romero, Isabel; Universitat de Girona, Chemistry Teixidor, Francesc; Institut de Ciencia de Materials de Barcelona, CSIC Vinas, Clara; Institut de Ciencia de Materials de Barcelona,

Icosahedral Boron Clusters: a perfect tool for the enhancement of polymer features.

R. Núñez,[a] I. Romero,[b] F. Teixidor[a] and C. Viñas[a,]*

[a] Institut de Ciència de Materials de Barcelona (ICMAB-CSIC), Campus de la U.A.B., E-08193 Bellaterra-Barcelona (Spain). Email: clara@icmab.es

[b] Departament de Química, Universitat de Girona, Campus de Montilivi, E-17071 Girona, Spain.

Key learning points

(1) The capability and improved features of both π conjugated and single bond polymers by boron clusters inclusion.

(2) The role of anionic boron clusters as doping agents to produce conductivity in Conducting Organic Polymers (COPs).

(3) A COP film can self-repair due to a metallacarborane doping agent bonded to the main chain of polymer.

(4) Boron clusters usually enhance desired properties in polymers.

(5) 1D-coordination polymers derivated of icosahedral carborane clusters with main group metals, d- and f-block elements.

Acknowlegment:

This work was supported by Generalitat de Catalunya (2014/SGR/149), and MINECO (CTQ2013-44670-R and CTQ2015-66143-P). C.V. thanks European Union (COST Action CM1302-Smart Inorganic Polymers).

Introduction

A polymer is a substance composed of macromolecules; a macromolecule being one of high relative molecular mass, with a structure comprising multiple repetition of units derived from molecules of low relative molecular mass . The word polymer comes from the Greek words Poly (meaning many) and meros (meaning parts). The molecular structure of the polymers can be linear, branched and cross-linked. The process by which monomers are linked to form polymers is called Polymerization. If the polymerization takes place without the elimination of any product, the process is called "addition polymerization", while the process is called "condensation polymerization" if small molecules are eliminated. A large number of organic, inorganic or organometallic compounds can be polymerized. Their physical, chemical and electrical properties depend on complex sets of interacting factors that include molecular structure, molecular size and cross-link density.

Of the many types of polymeric materials, π conjugated organic polymers have attracted much interest because their unusual properties lend themselves too many novel applications. Previously, organic polymers were considered good insulators. However, this concept was radically changed when it was shown that the conductivity of polyacetylene can be increased via doping by 13 orders of magnitude, up to about 10^4 Scm^{-1}. This class of polymers known as electrically conducting organic polymers (COPs) was discovered in 1977 by Alan J. Heeger, Alan G. MacDiarmid and Hideki Shirakawa,[1] who were awarded jointly the Nobel Prize in Chemistry 2000 "for the discovery and development of conductive polymers". This award stemmed from their work on conducting polyacetylene via doping with oxidants, which they carried out in the late 1970s. Although there is a large body of research on polyacetylenes, the

instability of many of these materials in air, until recently, limited the number of practical applications. While these studies produced the most dramatic results, investigations of conjugated polymeric materials date back to the early 1960s, with the first organic polymer of significant conductivity being polypyrrole (PPy) as reported by Donald Weiss and coworkers in Australia.[2] The development of polypyrrole materials is presented beginning with the first report of pyrrole's polymerization in 1915 through the more well-known work of Diaz and coworkers in 1979.[3]

Icosahedral boron clusters (Chart 1) display many particular characteristics that do not find parallel in their organic counterparts. The unique stabilities and geometrical properties of the isomeric icosahedral *closo* $C_2B_{10}H_{12}$ carboranes in their anionic and neutral forms as well as their exceptional properties, such as low nucleophilicity, unparalleled chemical inertness, electron-withdrawing character through the carbon cluster vertexes (C_c) substituent and adaptable hydrophilicity, inspired research on the development of new polymeric materials incorporating boron clusters. Cobaltabisdicarbollide [3,3'-Co(1,2-$C_2B_9H_{11}$)$_2$]$^-$ (**1**) which was synthesized in 1965[4] is the most intensively studied anionic borate cluster, has a great chemical stability, high molecular volume, low nucleophilic character and low charge density because the negative charge is distributed between 45 atoms.[5]

Icosahedral boron clusters are part of polymeric structures linked by C_c or by B atoms through covalent two-centered-two-electron (2c-2e$^-$) bonds. However, these clusters have the capacity to produce three-centered-two-electron (3c-2e$^-$) bonds, given the hydride character of the H atoms of the B-H vertexes. Thus, coordination polymers with icosahedral boron clusters as ligands are significant for their potential applications as well as for their structural chemistry perspective.

Since the discovery of polyhedral boranes in the early 1960's, new inorganic-organic hybrid boron cluster-containing polymers (polypyrrole, polythiophene, silane, siloxane-acetylene, polyaryl(ether), polyimides, ….) have been developed to combine, in a single polymeric system, the desirable features of inorganic materials such as high-temperature stability, hardness and chemical inertness with easy processability and high solubility characteristic of organic materials.

The trend towards miniaturization of devices and, at the same time improved performance, high reliability and easy to use, makes that electronic and semiconductor industries are constantly demanding more technically advanced and sophisticated materials. This review goal is aimed to present the current status of hybrid polymers incorporating icosahedral boron clusters and how the new polymers present enhanced properties. We are confident that the review will be of great practical value to both boron cluster scientists and researchers in other areas that are interested in exploring the possibilities of boron clusters. Hopefully it will also increasingly find its way into advanced teaching, showing the possibilities of boron clusters to the future new scientists.

I) Conducting organic polymers incorporating icosahedral boron clusters.

COPs are also known as "synthetic metals" because one of their potential applications is as substitutes for metals or inorganic semiconductors. COPs are promising materials for technological and biomedical applications due to their attractive electronic and optical properties. Conducting and reducing states of COPs can be easily electrochemically generated from the corresponding monomers. During the electropolymerization, anions from the solution are inserted into the polymer matrix to maintain the material's electroneutrality, neutralizing the positive charges generated in the oxidized polymer

threads (Figure 1). The COPs conducting state is the one requiring a doping agent and is produced by oxidizing the insulating material.

Doping agents play a relevant role on the stability, morphology as well as in the chemical and physical properties of the polymer. Therefore, the nature of the counter-ion used in the electropolymerization and the applied experimental conditions play a very important role in the resulting properties of the COP films. $[ClO_4]^-$, Cl^-, $[BF_4]^-$, $[PF_6]^-$ $[NO_3]^-$, surfactants such as dodecylbenzene sulfonate (DBS), dodecyl sulfonate, naphthalene sulfonate, and even counter-ions like heteropolyanions ($[SiW_{12}O_{40}]^{4-}$ or phosphotungstate $[PW_{12}O_{40}]^{3-}$), among others have been studied as doping agents. For practical applications, long-term stability of the material towards repetitive oxidation/reduction cycling or towards exposure to high anodic potential for short periods of time is of primary interest. A major obstacle to commercialization of COPs is the relatively poor stability of the COPs-based devices to several degradation mechanisms such as rapid oxidation by water or oxygen, with Joule heating or with volume change when the material oxidation state is changed electrochemically.[6]

The COPs chemical stability limit is known to be related to the overoxidation resistance limit (ORL) of the material, beyond which the conducting material properties are definitely lost. COPs have been made more resistant to overoxidation by doping with low nucleophilic, low electron density and low coordinating hydrophobic anions.

Boron clusters have been built into the electroactive polymers with the following main objectives: i) to play the role of doping agent (sections 1a and 3); ii) to modify the chemical composition of the COPs by the doping agent (section 1.1b) or iii) to incorporate boron into the polymer (sections 1.2b and 2). The first step to achieve the preparation of novel COPs covalently linked to neutral or anionic icosahedra boron cluster derivatives is the synthesis of the starting monomer derivatives covalently linked

to the corresponding boron cluster. The second step is the electropolymerization of these functionalized monomers to produce the corresponding COPs films.

1.- Polypyrrole materials containing icosahedral boron clusters.

Of the many COPs, the polypyrrole (PPy) is among the most popular. Chemical methods for the oxidative polymerisation of pyrrole had been known for many years, but a new era in the development of these materials arose when Diaz produced the first free-standing films of electrochemically deposited polypyrrole, poly-N-methylpyrrole and poly-N-phenylpyrrole on platinum electrodes in an $CH_3CN/[NEt_4][BF_4]$ solution.[3]

The electrochemical formation of conductive PPy films takes place by the anodic oxidation of pyrrole in CH_3CN at a moderate positive potential ($E_{1/2}$ = 1 to 1.3 V *vs* Saturated Calomel Electrode (SCE)). The initially formed radical species is immediately oxidized at the applied potential, since it is more oxidizable than the monomer, leading to a new radical cation. The continuing reaction is a lengthening of the oligomer chain. Since polymers from pyrrole have markedly lower oxidation potentials (0 to 0.4 V (SCE)) than the monomer, they are obtained in an oxidized state which is electrically conducting, allowing the growth of the film. The important point is that the resulting polymer contains mainly structural units linked via the of 2,5 positions of the pyrrole ring (Chart 2). Thus, non-substituted pyrrole at the 2,5 positions is highly recommended to produce good quality PPy films.

1a.-. Polypyrroles that incorporate boron clusters as doping agents of the electroactive polymers.

The first described PPy that incorporates anionic icosahedral boron clusters as doping agents was announced in 2000, when the PPy electrochemical synthesis of pyrrole (0.1 M) in the presence of 3.5 10^{-2} M in Cs(**1**), with 1% (v/v) water was reported.[7] Electropolymerization was performed in CH_3CN in a double compartment cell with a

standard three-electrode system; Pt, Pt wire and Ag/AgCl (0.1 M $[NBu_4]Cl$ in CH_3CN) were used as working, counter and reference electrodes, respectively. Sequential cyclic voltammograms for the electropolymerization of pyrrole in the presence of (**1**) displayed a continuous growth of the PPy(**1**) film after every new cycle proving the conducting nature of the formed material (Figure 2).[7] Besides, the anodic and cathodic semicycles present precisely well-defined peaks (Figure 2a). The PPy(**anion**) abbreviation would mean, through this review text, the polypyrrole polymer doped with the **anion** that appears in the parenthesis.

Due to the hydrophobicity, large size and multiple binding properties of the anion (**1**), its retention within the polymeric PPy(**1**) material is facilitated. Thus, the oxidation-reduction process, also called doping/undoping, occurs via de-insertion and insertion of cations (Scheme 1). The PPy(**1**) film is highly sensitive to the cationic volume of the solute, allowing to develop cationic selective membranes by control of the applied reducing potential (Figure 3). The chronocoulometries registered during the charge-discharge process show an almost perfect reversibility of the cation exchange process and no detectable degradation of the membrane due to (**1**) loss or overoxidation even after 40 successive cycles.

To study if PPy(**1**) interacted with the large cations of alkylammonium and phosphonium salts, cyclic voltammetry was performed on PPy(**1**) in either aqueous solutions of $[NR_4]Cl$, or $[PR_4]Cl$.[8] The materials were made of a conducting PPy(**1**) covered by a layer of well-adhered crystals of $[NR_4]^+$ or $[PR_4]^+$ salts that were observed by SEM. Although the layers resemble self-assembled monolayers (SAM), there are noticeable differences between the two types of surface coating particularly the cationic species participate in generating the layer even though there is no possible way to covalently bind the cations to the PPy surface. These stable layers, that can be made of

variable compactness, are the result of the formation of $[NR_4][(\mathbf{1})]$ or $[PR_4][(\mathbf{1})]$ salts that are highly insoluble in water. Figure 4 graphically shows the material. The films, which are unidirectional (inwards) cation barriers, are highly stable in aqueous media but are easily dissolved in CH_3CN in which the $[NR_4][(\mathbf{1})]$ or $[PR_4][(\mathbf{1})]$ salts are soluble.[8] This discovery can be of remarkable interest both as a new way to deposit crystalline materials layers on the surface of COPs films, but also as a way of producing defects on the surface by controlled removal of the doping anions.

Recently, the surface functionalization of a Pt electrode by the electropolymerization of pyrrole doped with the anionic *closo* ferrabisdicarbollide cluster, [3,3'-Fe(1,2-$C_2B_9H_{11})_2]^-$, (**2**), has been reported. As in the above described case of PPy(**1**) films, the doping agent (**2**) allows the PPy(**2**) to grow without limits increasing its conductivity after each cycle.

The in-depth uniform distribution of the doping anion (**1**) was unambiguously demonstrated in PPy(**1**) films by using X-ray photoelectron spectroscopy (XPS) analysis and Argon ion sputtering with no special experimental difficulties, thanks to the high boron content of the PPy(**1**). XPS measurements provided a surface polymer composition of $C_{5.3}N_1B_{4.15}Co_{0.23}$, corresponding to a PPy/(**1**) ratio of 4.3. Moreover, the high-energy N^+ shoulder is about 22% of the total N(1s) signal, in agreement with the previous results.7 Bearing in mind the above findings, further geometrical calculations confirmed the Py/(**1**) ratio stoichiometry. A graphical display of the ideal viewing of the PPy(**1**) layers is shown in Figure 5. The B-B diameter of the B-B longest distance in (**1**) is ≈ 11.0 Å including the two hydrogen atoms. Simple calculations performed on the unit $[H\text{-}Py\text{-}Py\text{-}Py\text{-}Py\text{-}H]^{2+}$, show that the farthest two carbon atoms are separated by ≈ 12.3 Å, relatively close to the axial H-(B)···(B)-H distance in (**1**). From a geometrical point of view, there is 4 pyrrole fragments per each (**1**) anion.[9]

PPy materials doped with the anionic icosahedral boron clusters: $[B_{12}H_{12}]^{2-}$ (**3**) and $[B_{12}I_{12}]^{2-}$ (**4**); [10] $[1\text{-}NH_3\text{-}B_{12}H_{11}]^-$ (**5**), $[1\text{-}NH(CH_2\text{-}C_6H_5)_2\text{-}B_{12}H_{11}]^-$ (**6**), $[1\text{-}NH(CH_2\text{-}C_{10}H_7)_2\text{-}B_{12}H_{11}]^-$ (**7**) and $[1\text{-}NH(CH_2\text{-}C_{12}H_{23})_2\text{-}B_{12}H_{11}]^-$ (**8**);[10] as well as monoanionic metallacarborane derivatives of (**1**): aryl (**9**)-(**12**),[10] polyether (**13**)-(**14**)[10] and polyTHF (**15**)-(**16**) were also reported to study on the influence of different composition (metallacarborane or borane), shape (*commo* bisdicarbollide or icosahedron) and charge (one or two) as well as different substituent (at the boron vertex or at the carbon one) of the doping icosahedral boron anions on the film growth and ORL value (Table 1). Charts 3 and 4 display the chemical structure of these anions.

The PPy film growth speed found was PPy(**1**)>PPy(**11**)>PPy(**12**)>PPy(**9**)>PPy(**10**). The materials with less tendency to grow are PPy(**13**) and PPy(**14**); their growth is one order of magnitude less than for PPy(**1**). When doping agents were (**13**)-(**16**), the conductivity decays dramatically after each new cycle until flattening the signal. This indicates higher difficulty in the materials' growth and consequently a very thin layer on the electrode. Polyether and polyTHF branches of the monomers (**13**)-(**14**) and (**15**)-(**16**) beam away from the surface, not allowing the deposition of new polymer layers, and so ceasing the material growth.

As SEM displayed different morphologies between PPy(**1**) and common anion doped PPy(**ClO_4**) and PPy(**PF_6**) membranes (Figure 6), the ORL and thermal resistance of these materials were studied.[10] ORL tests (Figure 7a) were carried out by Linear Sweep Voltammetry (LSV). A higher ORL value of PPy(**1**) material, approx. 300 mV, as compared to commonly used doping anions, (**DBS**) and (**PF_6**), was obtained. The PPy(**1**) overoxidation stability was attributed to the unique capacity of (**1**) to continuously compensate the moving positive charges in the COP layer (Figure 5). The tridimensional disposition of B-H's in (**1**) is ideal to cover all points in space, therefore

having the ability to completely compensate the cationic charge of the PPy film. ORL values of PPy(**1**)-PPy(**14**) membranes are summarized in Table 1.

Furthermore, Thermogravimetric Analysis (TGA) in inert atmosphere shows that the presence of (**1**) improves the thermal resistance of the PPy increasing both the temperature at which the weight lost begins (200ºC *vs* 130º C) and the weight lost up to 600ºC (22% *vs* 36%).[7]

The enhanced ORL and thermal properties of these PPy(**1**)-PPy(**14**) materials opened up significant opportunities for their application in practical devices. The fate of the doping anions before and during the polymer overoxidation processes was studied.[10] Figure 8 shows the XPS studies of plain, anodically processed, PPy(**7**) material and its overoxidized sample. The chemical composition on C and B of plain PPy(**7**) film remains unaltered throughout the whole thickness of the sample (Figure 8a).Conversely, its overoxidized sample (Figure 8b) shows two distinct regions: in the inner layers region (horizontal lines) boron atomic concentration is lower than its expected for a homogeneous overoxidized film whereas layers close to the solution membrane face (vertical lines) show a higher concentration. This can be understood as the movement of the doping anion during the overoxidation process from the inner layers (closer to the electrode) to the solution membrane face and in the case of PPy(**7**) as a result of its shape, an accumulation of (**7**) happens (Figure 9).[10]

1b.- Polypyrroles that incorporate boron clusters at the branches of the polymer.

Pyrrole derivatives covalently linked to carborane or metallacarborane clusters can be synthesized by bonding the substituent at the β carbon atoms of the pyrrole ring, 3-, 3,4-, or at the N- vertexes of the pyrrole ring (Chart 2).

1b.1.- N-substituted pyrrole units incorporating anionic closo cobaltabisdicarbollide.

Following the ring opening reaction,[4] pyrrole rings covalently bonded at the N- by a diether aliphatic chain to an anionic cobaltabisdicarbollide unit [3,3'-Co(8-C_4H_4N-$(CH_2)_2$-O-$(CH_2)_2$-O-1,2-$C_2B_9H_{10}$)(1',2'-$C_2B_9H_{11}$)]$^-$ (**17**) and [3,3'-Co(8-C_4H_4N-$(CH_2)_5$-O-1,2-$C_2B_9H_{10}$)(1',2'-$C_2B_9H_{11}$)]$^-$ (**18**) were obtained as pyrrole substituted synthons for COPs preparation.[11]

The polymerization of the anionic monomer (**17**) as well as its copolymerization with pyrrole units lead to the formation of a new group of self-doped PPy(**17**) and copolymer PPy(**17**):PPy,[5] improving the already outstanding properties previously described by PPy(**1**).[7] Figure 10 displays the proposed structure of PPy(**17**) and its copolymer PPy(**17**):PPy (1:4). As the doping agent is inherently bonded to the pyrrole unit in compound (**17**), no supporting electrolyte is necessary during polymerization. So, the electropolymerization of K(**17**) was carried out in dry CH_3CN by cycling the potential from –0.5 to 1.7 V *vs*. Ag/AgCl/[$N(C_4H_9)_4$]Cl (0.1M CH_3CN). Figure 11(a) shows the growth of PPy(**17**). Copolymerization of (**17**) with pyrrole monomer (ratio 1:1) was carried out under the same conditions indicated above (Figure 11b). Higher current intensities and a lower half wave potential were found in the copolymer PPy(**17**):PPy with respect to the polymer PPy(**17**), suggesting the existence of longer chains and a better packing of polymeric chains in the copolymer PPy(**17**):PPy. As it is known, the introduction of large groups into the pyrrole ring at the N- or 3- position usually brings about a drop in the conductivity and an increase of the band gap due to the steric hindrance to planarity of the conjugated system.[5] This is not the case of (**17**). The conductivity of thin PPy(**17**) films and PPy(**17**):PPy copolymer was measured by the four-point probe method and was found to be 1 and 9 Scm^{-1}, respectively.[5] Common anion doped PPy(**Cl**) or PPy(**ClO_4**) prepared under the same conditions show conductivities in the same order of magnitude than the copolymer.

Combining plasma argon ion sputtering and XPS, it was found that the PPy(**17**) composition is practically constant through the whole depth of the material indicating the absence of chain defects during electrochemically film growth and that one charge carrier exists nearly every four pyrrole units (N^+/N_{total} ratio ~0.25) as for PPy(**1**).5 The amount of K^+ found in the polymer matrix was negligible so, the three fold excess of (**17**) anions were compensated by H^+ generated during the polymerization process that were trapped into the PPy(**17**) film (Figure 10).

ORL experiments of self-doped copolymer PPy(**17**):PPy do not visualize a clear maximum suggesting an extraordinary increase of its overoxidation resistance (Figure 7a).[5] Thus, for compositionally similar materials, copolymer PPy(**17**):PPy and PPy(**1**), the fact that (**1**) is grafted to the PPy strand allows copolymer PPy(**17**):PPy go far beyond the overoxidation limit of the PPy(**1**) that has no anion grafting. The self-doped copolymer PPy(**17**):PPy is the best PPy material in terms of overoxidation resistance. Copolymer PPy(**17**):PPy can be one remarkable example of self-repairing materials because the material really do not die upon overoxidation because reversible overoxidized ↔ reduced process is permitted and in the case that the overoxidation threshold was surpassed the material would react to restore itself (Figure 7b).[12] This unique behavior is due to grafting of the cobaltabisdicarbollide (**1**) to the PPy but also on the nature of the anion.[12]

Because monomer (**17**) had inhibited the polypyrrole backbone oxidation in the films of PPy(**17**), copolymerization of monomer (**17**) with the cationic water-oxidation catalyst $[Ru_2(\mu\text{-bpp})(\mathbf{ttpy})_2(H_2O)_2]^{3+}$, (bpp= bis(2-pyridyl)pyrazolato anion and **ttyp**= 4'-(*p*-pyrrolylmethylphenyl)-2,2':6',2''-terpyridine), was done by electropolymerization of solutions containing a 1:1 molar ratio of both monomers in fluorine-doped tin oxide electrode (FTO).[13] The ratio of monomers incorporated into the PPy backbone of the

material was evaluated by UV/Vis spectroscopy and turned out to be roughly 1:1, indicating that the rate of polymerization of both monomers is practically the same. The new generated material, copolymer PPy(**17** and $[Ru_2(\mu\text{-bpp})(ttpy)_2(H_2O)_2]^{3+}$) on FTO surface, is capable of oxidizing water to molecular dioxygen with a turnover number (TN) of 250. This value represents the best performance ever obtained in a heterogeneous phase using a chemical oxidant.[13]

1b.2- C-substituted pyrrole synthons bonded to carborane clusters.

3- and 3,4- Pyrrole derivatives covalently linked to a neutral *closo* or anionic *nido o*-carborane via a methylene or ethylene spacer have been synthesized. These synthons (see Chart 5) are the following: i) neutral mono substituted (**19**),[14] (**20**),[14] (**21**),[15] (**22**);[15] ii) neutral di substituted (**23**),[16] (**24**)[15] and iii) anionic mono substituted compounds (**25**),[14] (**26**).[14]

The first conducting polymer funtionalized with covalently linked carborane units was obtained by anodic oxidation of the substituted (**19**) pyrrole monomer in 10^{-1} M $[NBu_4][PF_6]$ anhydrous CH_3CN.[17] The electrosynthesis of PPy**20**(**PF_6**) films was carried out from 10^{-2} M solution of (**20**) in the same conditions. Monomer (**20**) that presents an ethyl group spacer was more efficiently electropolymerized than (**19**) with a methylene group. The charge transport mechanism across the films was controlled by the diffusion of (**PF_6**) counteranions. The resulting electroactive PPy**19**(**PF_6**) and PPy**20**(**PF_6**) films exhibit strongly increased overoxidation resistance, about 120[17] and 300[14] mV respectively, shifted towards more positive potentials compared with plain PPy(**PF_6**). The conductivity ($\sigma \sim 10^{-1}$ S cm^{-1}) of PPy**19**(**PF_6**) polymer, measured at room temperature by the four-probe method, is 2-3 orders of magnitude lower than that of other 3-monosubstituted polypyrroles.[17] These electrochemical characteristics were directly attributable to the presence of the carboranyl moiety: its increased ORL is due

to the electron-withdrawing character of the carboranyl unit while decreased conductivity is a consequence of the steric bulkiness of carborane cluster, which would produce conformational constraints in the conjugated backbone decreasing its mean conjugation length.[17]

Moreover, these PPy**19(PF$_6$)** and PPy**20(PF$_6$)** materials were more thermally stable than PPy(**PF$_6$**); only 15% loss in the mass was found for PPy**19(PF$_6$)** at 700ºC while a continuous mass loss till 70% was observed for PPy(**PF$_6$**). The improvement was attributed to the oxidation of B-H vertexes of the carboranyl cluster to the more thermally stable B-O-B groups.[14]

The oxydation of the (**21**) and (**24**) monomers led to the formation of the PPy**21(PF$_6$)** and PPy**24(PF$_6$)** films. The disubstituted 3,5-pyrrole (**24**) and its corresponding PPy**24(PF$_6$)** polymer were oxidized at more positive potential than the substituted 3-pyrrole (**21**) and its conforming PPy**21(PF$_6$)** membrane due to the presence of two sterically hindered carborane clusters at the 3,5- vertexes of the pyrrole ring (Table 1).

However, when comparing PPy**23(PF$_6$)** and PPy**24(PF$_6$)**, the poly(3,4-diphenylpyrrole) PPy**24(PF$_6$)** was found to be more easily oxidizable which indicates a more conjugated structure, as was also supported by the UV-vis spectroscopy data.[15] The monosubstituted monomer (**22**) that contains two carboranyl clusters did not yield a conducting polymer deposit even under a different set of experimental conditions (oxidation potentials, solvents, monomer concentration, among others), possibly due to the high steric hindrace of dicarboranylmethylphenyl substituent at the 3- position of the pyrrole ring.[15]

In contrast with the feasible anodic electropolymerization of the neutral carboranyl pyrrole units, the anionic pyrrole synthons (**25**),[14] and (**26**) were found to not electropolymerize at the tested experimental conditions.[14] At 0.1 Vs^{-1}, two closely

spaced irreversible redox processes were seen for both monomers (0.50 / 0.82 V and 0.48 / 0.75 V, respectively *vs* Ag/Ag^+ 10^{-2} M). For the first redox system, the number of electrons involved in the rate-determining step was two while in the second redox process the results were perfectly consistent with a one-electron transfer.[14] While the nature of these two irreversible redox systems was not fully elucidated, their low values are consistent with the oxidation of the anionic *nido* carboranyl cluster because the oxidation of the pyrrole unit requires higher potentials. In addition, no visible film was detected on the electrode surface in the range 0.8 to 1.5 V *vs* Ag/Ag^+ 10^{-2} M.[14]

It is to be noticed the ability of the anionic N-substituted pyrrole (**17**) to electropolymerize, in contrast with the non electropolymerization of the anionic pyrrole synthons (**25**),[14] and (**26**) described below.[14]

2.- Polythiophene materials containing icosahedral boron clusters.

Thiophene is a heterocyclic compound (Chart 2) consisting of a flat five-membered ring. Polythiophene polymer (PTh) is formed by linking the monomers through their 2,5 positions and become electrically conductive upon partial oxidation. The current thiophene derivatives (Chart 6) incorporating neutral *closo* or anionic *nido* carborane cage covalently linked to 3- or 3,4-thiophene moieties or via a phenyl spacer arm are the following ones: i) neutral mono substituted (**27**),[15] (**28**);[15] (**30**), (**31**), (**32**);[18] (**34**);[19] and ii) anionic mono substituted (**29**)[15] and (**33**).[19]

Efficient electropolymerization of neutral (**30**), (**31**) and (**32**) monomers was run in CH_2Cl_2 + 0.2M $[NBu_4][PF_6]$. As the (**30**)-(**32**) units have one α ring carbon directly linked to the C_c of carborane cage, the PThs**30**(**PF_6**)-PThs**32**(**PF_6**) COPs contain the carborane clusters in the polymer backbone. These polymers show high thermal and electrochemical stabilities compared with parent PThs. The PThs**30**(**PF_6**) has the highest doping level, which is associated with the formation of the largest population of

bipolaron charge carriers that largely reduces the π-π*band gap and provides the highest conductivity of these family of materials. In the insulating form, PTh**30**(**PF_6**)-PTh**32**(**PF_6**) films display optical features at 528, 488 and 425 nm, respectively. PTh**30**(**PF_6**) shows well defined fine structure of high conjugation.[18]

There is no effect on the electroactivity of PTh**27**(**PF_6**) and PTh**28**(**PF_6**) when highly oxidizing potentials were applied.[15] No COPs were generated from monomers (**29**), (**33**) and (**34**).[19] Polythiophene films, PTh**35**(**PF_6**) and PTh**36**(**PF_6**), containing in-chain (**1**) covalently linked to two bithienyl and terthienyl units were prepared by electropolymerization in CH_3CN. These films display redox processes attributed to the p-doping/undoping of the expected quaterthienyl and sexithienyl segments at ca. 0.8 V *vs* SCE. PTh**35**(**PF_6**) and PTh**36**(**PF_6**) display a more extended degree of conjugation than the parent oligothiophenes indicating a significant electronic delocalization through the cobaltabisdicarbollide cluster. These materials were efficient for the electrocatalytic reduction of protons to H_2 suggesting that could be robust and efficient catalysts.

3.- Poly(3,4-ethylenedioxythiophenes) containing icosahedral boron clusters.

Conductive polymers like poly(3,4-ethylenedioxythiophene) (PEDOT) are very attractive for their outstanding properties: extremely stable and highly conductive state; high transparency (90% at d = 100nm) and flexibility; high chemical and thermal/UV stability; easy processing by polymer dispersion as ready-to-use formulations mixed with solvents and additives or "*in-situ*" monomer polymerization for industrial scale production.

Commonly, monomer ethylene dioxythiophene (EDOT) is synthesized into polymer (PEDOT) through oxidation polymerization (Scheme 2).

Despite, the outstanding physico-chemical applications of PEDOT doped as a COPs, it is notable the lack of studies of PEDOT either with metallacarboranes or carboranes.

The first report on PEDOT(**metallacarborane**) was published in 2006.[20] The electropoly-merization of EDOT on Indium tin oxide (ITO) from Cs(**1**) in CH_3CN solution gave the polymer PEDOT(**1**) that is accompanied by a reversible oxidation of the doping anion. It results in a *p*-doped polymer embedded with short-chain reduced oligomers, as proven by the material composition, morphology, electrochemical and spectroelectrochemical behavior. The ratio between the numbers of EDOT molecules entrapped in the polymer *vs*. the oligomers is 0.88. This ratio was estimated from the doping level of the material considering that only the polymer can be doped. Its oxidation/reduction process takes place reversibly in the potential range –0.8/+0.7 V *vs*. SCE and is accompanied by cation exchange due to the non-extrudable character of the doping anion (**1**). It was also shown that an important oligomeric fraction is embedded in the main polymer.[20]

Recently, new electrochromic copolymers of EDOT and 1,7-(2'-$SC_4H_3)_2$-1,7-carborane (**31**) were synthesized, characterized and their electro-optical properties reported.[21] Several copolymers PEDOT(**31**):PEDOT were successfully prepared from various monomer feed ratios by electropolymerization. Electrochemical and optical properties of the copolymers can be adjusted by playing with monomer feed ratios; the maximum wavelength of PEDOT at 600 nm can be shifted to lower values (i.e., 522 nm) by increasing the ratio of (**31**) in the monomers mixture. The copolymer films showed electrochromic properties: purple when reduced and transparent sky blue when oxidized. Also, during redox switching the films exhibited a percent transmittance change between 32% and 46% with a switching time between 1.0 s and 1.3 s.[21]

II. Photoluminiscent carborane-containing π-conjugated polymers.

All conjugated polymers possess extended π conjugation through the molecular backbone alternating double- and single-bonds that produces a delocalization of the π

electrons across all adjacent aligned *p*-orbitals. Single and double bonds become similar and π-electrons can be readily moved from one bond to the next, what makes conjugated polymers to be one-dimensional semiconductors. Excitation energies of conjugated π electrons are usually in the visible range and they are, therefore, addressed as being optically active. One of the drawbacks for these π conjugated polymers is the extended conjugation through aromatic moieties that causes a tendency to bundle and π-stack. These phenomena influence the processability and stability of such systems, which is a problem for their utilization in optoelectronic devices. The incorporation of carborane clusters into the polymers' backbone or branches aids to confer solubility and stability, while altering their luminescent properties.

1. Carborane-containing *p*-phenylene-ethynylene-based polymers (PPE).

Several examples of molecular π conjugation of icosahedral $[CB_{11}Cl_{10}]^-$ clusters and *exo*-2D π systems have been recently reported.[22],[23] Different families of π-conjugate polymers containing *o*-, *m*- and *p*-carborane (Chart 1) in the backbone have been reported during the last years.[24] The incorporation of aromatic and carboranyl groups into the backbone produces a stabilizing effect but, additionally, linear π-conjugate aryl-ethynyl-carborane polymers exhibit photoluminescent properties.

π-Conjugate polymers **32a-d**, **33a-b**, **33e-f** and chiral π-conjugate polymers **32g(R)-33g(R)** and **32g(S)** were synthesized from the reactions of monomer bis(4-iodophenyl)-*o*-carborane or bis(4-iodophenyl)-*m*-carborane with the corresponding *p*-phenylene-ethynylene derivatives by a Sonogashira-Hagihara coupling polycondensation reaction (Scheme 3a). Polymer **34**, in which the *p*-phenylene-ethynylene units are bonded at B9 and B12 atoms, was also prepared (Scheme 3b). The number-average molecular weights (M_n in $gmol^{-1}$) of **32a-d**, **32g(R)** and **32g(S)** were 2800, 3100, 4100, 3200, 3800 and 3000, respectively, whereas polymers **33a-b**, **33e-f, 33g(R)** and **34** displayed higher

molecular weights of 26600, 27600, 36400, 31200, 29800, respectively. The obtained polymers were soluble in organic solvents such as THF, $CHCl_3$, CH_2Cl_2 and toluene.

Polymers **32a-c** and **32g(R)** were not fluorescent in THF solutions due to an intramolecular charge-transfer (CT) process from the electron-donating *p*-phenylene-ethynylene units to the antibonding orbital of the C_c-C_c bond in the *o*-carborane. Contrary, their homologous with *m*-carborane **33a-b, 33e-f** and **33g(R**), as well as polymer **34** show intense blue emission in $CHCl_3$ (Table 2). In **34**, the inclusion of substituents at the B vertexes of the *o*-carborane cluster does not cause any structural change in the excited state of the *p*–phenylene-ethynylene moiety so its luminescence is not affected. Nevertheless, polymers **32a-c** and **32g(R)** exhibited orange emission in suspensions of THF/H_2O, 1/99 (v/v) (Table 2), that was originated from aggregation-induced emission (AIE). Additionally, **32g(R)** and **33g(R)** films showed fluorescence emission bands at 562 nm (Table 2), indicating that the carborane unit prevents the stacking of π-conjugated main chains.

Following the same Sonogashira–Hagihara polycondensation procedure aromatic ring-fused carborane-based π-conjugated polymers **35a** and **35b** were synthesized (Scheme 4).[25] Contrarily to polymers **32a-c**, **35a** and **35b** exhibited intense blue luminescence in THF solution (Table 2). The introduction of benzocarborane has little effect on the intramolecular cage-π interaction in the excited state, thus the carborane cage acts as a simple electron-withdrawing group without disturbing the emission of π-conjugated systems.

Polymer **37** was also synthesized by complexation of ligand **36** with $Zn(OAc)_2{\cdot}2H_2O$ *via* Sonogashira–Hagihara coupling reaction (Scheme 5).[26] While monomer **36** was not luminescent in solution, polymer **37** exhibited fluorescence with an emission maximum at 465 nm (Table 2).

Polymers with the structure of **38** were obtained by the reaction of *nido*-decaborane ($B_{10}H_{14}$) with poly(*p*-phenylene–ethynylene) polymer in different ratios (0.05, 0.10, 0.20, 0.40) (Scheme 6). The M_n of **38** decreases from 4600 to 3200 with increasing feed ratio.[27] These polymers showed light blue emission in THF, whereas in the solvent mixture THF/H_2O, 1/99 (v/v) the emission maxima was red-shifted to 529 nm, indicating a shortening of the effective π-conjugation length due to the introduction of carborane clusters (Table 2). Furthermore, the introduction of the *o*-carborane clusters into the polymer main chain led to a high thermal resistance and an improvement in ceramic yields on thermolysis to 1050 ºC.

More recently, the polymerization of benzocarborane[2,1-b:3,4-b']dithiophene (**39**) to give polymers **40** and **41** with the aromatic ring fused to the carborane cluster has been reported (Scheme 7).[28] These polymers showed excellent thermal stability with T_{d5}, that is the temperature at which the polymer losses 5% of its weight, at above 375 and 400 ºC, respectively. Absorption data of **40** and **41** in solution and films are in Table 2. The ionization potential of these polymers were 5.0 and 5.4 eV, slightly larger than polymers without carboranes, indicating that the cluster acts as an inductive electron-withdrawing comonomer.

2. Carborane-containing polyfluorene polymers.

In 2009, *p*- and *o*-carborane-containing polyfluorene polymers **43** and **45a** were synthesized from **42** and **44**, respectively, using a Yamamoto type Ni(0) dehalogenative reaction in the presence of [Ni(COD)$_2$] (Scheme 8).[29] Later, polymer **45b** was accomplished via a Stille coupling reaction as shown in Scheme 8.[30] The thermal analysis of polymers **45a** and **45b** showed a glass transition temperature (T_g) between 128 and 137ºC.

Polymer **43** exhibits blue emission in $CHCl_3$, whereas the presence of *o*-carborane into **45a** gave an additional second band, red-shifted, at around 565 nm (Table 2), which suggested that the electron-withdrawing *o*-carborane is in conjugation with the backbone system; then the energy absorbed by the fluorene units is transferred to the *o*-carborane cluster and emitted in the orange region (Table 2). Furthermore, carborane-containing polymers **45a** and **45b** showed blue-shifted emission in the solid state compared to the solution state that was attributed to forced aggregation of adjacent fluorene segments (Table 2). Contrarily to poly(dihexylfluorene), annealing studies on **43** films showed a minimal increase in green emission after heating to 180 ºC in air for 2 h. *o*-Carborane suppresses the green emission that commonly plagues blue-emitting polyfluorene systems. The fluorescence spectrum of **45a** in solid-state displays a green emission centered at 520 nm that seems caused by excimer formation due to aggregation. After annealing in air at 180 ºC for 2 h, the films showed no shift in the emission wavelength but increased in intensity, which is likely a result of increased aggregation from rearrangements above T_g.

In parallel, two different polyfluorenes bearing pendant silylcarboranes **47** and **48** were prepared by homopolymerization or copolymerization of the monomer **46** by microwave-assisted Yamamoto nickel-mediated aryl-aryl coupling reaction (Scheme 9).[31] The M_n was found to plateau at ~7000 g/mol for all polymers obtained in the temperature range 10-150 ºC. Emission spectra of the thin films of **47** before and after annealing for 3 h at 160 ºC indicated that the fluorescence emission maximum was blue-shifted with respect to conventional fluorenes (Table 2), with a decrease in intensity when increasing carborane content. The presence of pendant carborane clusters elevates T_g and hinder chain packing, increasing stability and color purity, two essential properties for display materials.

Photoluminescent but no π-conjugated polynorbornene copolymers with pendant carbazoles and phenyl- (**49**) or methyl-*o*-carboranes (**50**) were synthesized as described in Scheme 10.[32] These copolymers possess high thermal stability and glass transition temperatures, T_{d5} > 410 ºC and T_g > 350 ºC, respectively. Due to the carbazole group, polymer **50** exhibits emission bands at around 351 nm and 366 nm, whereas polymer **49** that contain Ph-*o*-carborane shows a quenching of the fluorescence as a result of photoinduced CT process from the donor (carbazole) to the acceptor (Ph-*o*-carborane). Contrarily, when polymer **49** was treated with KOH/EtOH to produce the partial degradation of the cluster, the quenching process is blocked, and the material shows fluorescence emission.

III. Carborane-based polymers with other organic linkers.

Hybrid organic-inorganic polyaryl(ether-ketone)s containing aromatic rings and *o*- or *m*-carborane clusters in the main chain were synthesized using a typical superacid-promoted polycondensation reaction between bis(4-phenoxyphenyl) derivatives of *o*- or *m*-carborane and aromatic or aliphatic dicarboxylic acids.[33] Scheme 11 displays the preparation of polymers **51** starting from a *m*-carborane derivative. Polymers were obtained in high molecular weights (M_w > 150.000). These materials are amorphous and readily soluble in organic solvents, to give solutions from which strong and transparent films may be obtained. These polymers showed very high mass-retention on thermolysis: up to 93% and 97% under N_2 or air, respectively.

Soluble *m*-carborane polyimide polymers such as **52** and **53**, which possess different type of structures, were prepared according to Scheme 12 in moderate molecular weight from 10000 to 24000 g mol^{-1}.[34] These polyimides are non-crystalline materials; this is attributed to the bulkiness of the *m*-carborane cluster that disrupts intermolecular interactions and hinders regular and dense chains packing. The introduction of the *m*-

carborane greatly increases their thermal stability, in which T_{d5} values exceed 600ºC in N_2 and 100 ºC in air.

A polystyrene polymer containing *o*-carborane components covalently linked to the side chain was prepared by the Cu^I-catalyzed Huisgen-type "click" reaction between the azidomethyl-appended polystyrene polymer **54** and the ethynyl-terminated carborane leading to polymer **55** (Scheme 13).[35] The carborane-appended styrenyl polymer has a polydispersity index (PDI) of 1.52 and good thermal robustness.

The *p*-carborane-containing polymer **56** was synthesized by following the procedure displayed in Scheme 14.[36] Polymers **56** were dendronized using a divergent approach to introduce aliphatic polyester dendrons (generation 1 to 4) grafted to the polymer branches backbone to yield the dendronized polymer **57**. This approach afforded a maximum degree of dendronization of 70%. To increase the degree of dendronization, a first-generation macromonomer was polymerized using NMP to yield a fully functionalized first-generation dendronized polymer, which was then dendronized up to the fourth generation. Both approaches produced water-soluble dendronized polymers (1 mg/mL in pure water) with high molecular weights (in excess of 70 kDa), with potential biomedical applications, a narrow molecular weight distributions and a polydispersity index (PDI) < 1.1.

Amphiphilic carborane-containing diblock copolymers represented by polymer **58** were synthesized from 1-$OH(CH_2)_3$-2-$SiMe_2$*t*Bu-1,2-$C_2B_{10}H_{10}$ following the procedure described in Scheme 15.[37] The diblock copolymers were obtained by sequential addition of the silyl-protected oxonorbornene imide carborane derivative and Boc-protected oxonorbornene imide amine in different molar ratios. These copolymers were obtained with molecular weights ranging from 17 to 65 kg/mol and high PDI from 1.09 to 1.15.

IV.- Icosahedral boron clusters-containing silane and siloxane-polymers.

Besides the previous polymers, a large family of hybrid organic-inorganic polymers is formed by silane and siloxane-based polymers.4 The report of the first siloxy-*m*-carborane polymers dates back to the 1960s with the development of commercial DEXSIL and UCARSIL polymers used as stationary phases for high-temperature gas chromatography compounds. In the 70's of the last century, Donald D. Stewart reported different methods to obtain linear high molecular weight D2-*m*-carborane siloxanes with molecular weights up to (> $l0^6$). The ultra-high molecular weight polymers exhibited improved thermal and mechanical properties as a result of increased chain entanglement of the polymer chains.[4]

Later, a series of carborane-siloxane-acetylene polymers with outstanding exceptional thermal and oxidative degradation properties were developed. Polymers **59** and **60** were synthesized from 1,7-$(SiMe_2OSiMe_2Cl)_2$-1,7-$C_2B_{10}H_{10}$ following the procedure shown in Scheme 16. Thermal cross-linking of **59** produces a thermoset that gave a ceramic material in high yield after pyrolysis at 1000ºC. Polymer **60** exhibits high thermal stability, with weight retention of 78% at 1000 ºC, when compared with other ferrocenyl-siloxane polymers.[4] To develop high temperature elastomers upon thermal curing, a set of *m*-carborane-trisiloxane-diacetylene copolymers were prepared varying acetylenic frequencies in the backbone, with trisiloxane:carborane:diacetylene molar ratios of 10:9:1, 5:4:1 and 3:2:1. Variation in the copolymer sequence caused noticeable differences in the calorimetric glass transitions for those in which the diacetylene group was most concentrated.[38]

More recently, elastomeric *m*-carborane-siloxane polymers **61** have been prepared via rapid Karstedt-catalyzed hydrosilylation reaction using a branched siloxane crosslinker monomer (Scheme 17).[39] The elasticity of polymers can be modulated by careful choice

of the crosslinkers. The obtained polymers show an oxidative stability up to 300 ºC and their T_{d5} are in the range 500-550 ºC.

Poly(carborane-siloxane arylacetylene) polymers **62** and **63** were synthesized from the 1,7-$(SiMe_2OSiMe_2Cl)_2$-1,7-$C_2B_{10}H_{10}$ monomer and Grignard derivatives (Scheme 18).[40] Their thermal treatment results in a fully crosslinked thermoset by 500 ºC as a consequence of cycloaddition reactions involving the acetylene and aryl functionalities and subsequent formation of bridging disilylmethylene entities. The developed polymers have exceptional thermo-oxidative properties similar to their diacetylene counterpart poly(carborane-siloxane-acetylene) and enhanced mechanical properties for the thermoset samples when compared to the poly(siloxane-acetylene).

Polymers **64** were prepared by polycondensation reaction of 1,4-dilithiobutadiyne with 1,4-bis(dimethylsilyl)benzene and 1,7-$(SiMe_2OSiMe_2Cl)_2$-1,7-$C_2B_{10}H_{10}$ varying the molar ratios as follows: 100:0, 75:25, 50:50, 25:75 and 0:100 (Scheme 19).[4] These polymers were viscous liquids or low melting solids at room temperature and show good solubility in different solvents, such as THF, acetone, diethyl ether and chloroform. These polymers show good thermal stability giving high char yield (79-86%) when heated to 1000 ºC under N_2. Aging studies performed at elevated temperatures in air on a thermoset and a ceramic showed that these systems have excellent thermal and oxidative stability.

A series of poly(silylene-arylacetylene)s and poly(siloxane-arylacetylene)s with *o*-carborane in the backbone were prepared by the coupling reaction between the corresponding poly(silylene-arylacetylene) (PSA) or poly(siloxane-arylacetylene) (PSOA) and decaborane ($B_{10}H_{14}$) with different molar ratios ($B_{10}H_{14}$/PSOA: 0.6, 1.2, 1.8, 2.4) (Scheme 20).[41] The resulting carboranyl-containing PSOA polymers **65** could be converted into a thermoset below 250 ºC. The thermosets from carboranyl-contaning

PSA exhibit excellent thermal and thermo-oxidative stabilities with 91.5% residue yield in N_2 and 95.8% in air at 800ºC, whereas thermosets from polymer **65** exhibit oxidation-resistance with over 85% residue yields at 1000 ºC in air.

The use of 1,7-$(SiMe_2OSiMe_2Cl)_2$-1,7-$C_2B_{10}H_{10}$ as starting material in previous poly(carborane-siloxane-diacetylene) polymers **59-60** and **62-64** has limited their research due to the difficulties in obtaining it. This forced to synthesize other kind of polymers such as the poly(carborane-silanec) (**66**), which was obtained by the procedure displayed in Scheme 21.[4] These polymers are viscous liquids at room temperature with a molecular weight distribution with a PDI of 1.67 and Mn of 2853 g/mol. Polymers **66** show very good solubility in common organic solvent (THF, diethyl ether, and acetone), offering good processability to fabricate composites. Thermoset exhibits excellent thermal and oxidative property. The Td_5 is 762 ºC and char yield is 94.2% at 800 ºC in N_2, whereas T_{d5} is greater than 800 ºC and char yield is 95.6%, at 800 ºC in air. After pyrolysis, the char has no additional weight loss up to 800 ºC in air. Therefore, polymer **66** offers better mechanical and thermal stability than poly(carborane-siloxane-diacetylene) polymers, making the former suitable candidate as a matrix resin for advanced composites and as a precursor for ceramics, whereas the latter can be applied for high temperature elastomer.

Carborane-silane-acetylene polymers **67** and **68** have been prepared by hydrosilylation reaction of diethynylbenzene-silene polymers and 1,7-$[HSi(Me)_2]_2$-1,7-$C_2B_{10}H_{10}$ or 1,7-$[HSi(Ph)_2]_2$-1,7-$C_2B_{10}H_{10}$ (Scheme 22). Polymers possess a weight-average molecular weight of M_w = 21600.[42] In air, no weight loss up to 600 ºC occurs with a ceramic yield of up to 95% at 800 ºC, whereas under N_2 the polymer had high performance with ceramic yields more that 90% at 800 ºC. These polymers exhibit high mechanical and thermal stability as well as flame retardant properties. Additionally, the polymer

possesses a relatively high strength with flexural modulus of 1.86 GPa and 0.95 GPa at room temperature and 250 ºC, respectively.

V. Coordination polymers incorporating icosahedral boron clusters.

Coordination polymers (CP), are infinite multidimensional (1D linear or twisted chains, 2D squares and polygons and 3D cubes and polyhedra) materials with highly ordered structures. These structures are highly conditioned by the nature of multifunctional ligands and the coordination requirements of the metallic centres or the counter-ions. A slight modification in any of these factors can originate new structures and consequently new properties. The presence of metal-ligand association can lead to suitable materials with a particular usefulness or applicability; the metal can provide redox and magnetic properties among others and the appropriate ligand may determine the functionality of the material. On the other hand, polynuclear metal complexes attract great interest owing to their relevance to many important naturally occurring processes. The cooperative action of closely coupled dinuclear or multinuclear centers is required for several enzymes to carry out their biological functions as for example in the photosystem II. In this sense, the further design and construction of new supramolecular assemblies as models of the oxygen-evolving centre (OEC) can facilitate the understanding of the water molecules role in the catalytic process of water splitting.

Borane and carborane clusters are ligands of great interest in supramolecular chemistry because of their particular properties,[4] that may induce unconventional properties in the supramolecular structures in which they are inserted. Even though boron clusters are considered as weak coordinating compounds, it has been demonstrated that they can form supramolecular polymeric structures not only due to the bridging of polymetallic centers by various non-boron ligands, but also via so-called halogen or dihydrogen bonding of polyhedral clusters. The literature has accepted the use of the term

"coordination polymer" where B-H···M interactions are the primary interactions in the polymeric structures.

This section of the review summarizes 1D-coordination polymers derivate of icosahedral anionic *closo* $[CB_{11}H_{12}]^-$ and *nido* $[C_2B_{10}H_{12}]^{2-}$ clusters, with special emphasis in the polymeric structures of metallaboranes and carboranes of main group metals, d- and f-block elements. During the writing of this work, C.E. Housecroft published a review on carborane coordination polymers with transition metals;[43] therefore in this section we will only supplement this review with several new 1D-polymeric structures.

1.- Polymers with main group metals.

Neutral *closo o*-, *m*- and *p* carboranes are reduced by Group 1 metals. This reaction always results in the complete cleavage of the cage C_c-C_c bond, leading to the formation of "carbons-apart" *nido* $[R_2C_2B_{10}H_{10}]^{2-}$ isomers. Chart 7 displays the different positional isomers of 12 vertexes *nido* carboranyl ligands that are involved in these coordination polymers. As a consequence of their high stability, these clusters are very useful synthons for the production of numerous metallacarboranes of s-,p-,d-and -f elements. To force the two cage carbon atoms of the starting *closo o*-carborane to remain adjacent, "carbons-adjacent", during the reduction process, the most effective way is introducing a short linkage, $C_6H_4(CH_2)_2$ or $(CH_2)_3$, between the two cage carbon atoms of the icosahedral *closo o*-carborane cluster.[4]

Polymeric structures of Group 1 salts have been obtained during the reduction of the corresponding *closo*-carboranes 1,2-Ar$(CH_2)_2$-1,2-$C_2B_{10}H_{10}$[44] (Ar= *o*-C_6H_4, 1,8-$C_{10}H_6$, 1,1'-C_6H_4) and 1,2-R-1,2-$C_2B_{10}H_{10}$,[45] R=$(CH_2)_5$, $(CH_2)_6$, with excess of Na, K or Li metal in THF. The Group 1 metal polymers $[\{\mu$-1,2-[*o*-$C_6H_4(CH_2)_2$]-1,2-$C_2B_{10}H_{10}\}_2\{Na_4(THF)_6\}]_n$ **(69)**, and $[\{\mu$-1,2-[*o*-$C_6H_4(CH_2)_2$]-1,2-$C_2B_{10}H_{11}\}\{K(18$-

crown-6)$_2$}]$_n$ **(70)** maintain the two carbon atoms adjacent after the reduction process.[44] However, [{μ-1,4-[1,1'-(C_6H_4)$_2$-2,2'-(CH_2)$_2$]-1,4-$C_2B_{10}H_{10}$}$Na_2(THF)_3]_n$ (**71**)[44], [{1,3-(CH_2)$_5$-1,3-$C_2B_{10}H_{10}$}{$Na_2(THF)_4$}]$_n$ **(72)** and [{1,4-(CH_2)$_6$-1,4-$C_2B_{10}H_{10}$}{$Na_2(THF)_4$}]$_n$ **(73)** polymers[45] present "carbons-apart" 12 vertexes *nido*-carborane ligands as result of the complete cleavage of the C_c-C_c bond. The ^{1}H-, ^{13}C- and ^{11}B-NMR spectra of the polymeric compounds show the presence of methylene protons at the bridges in the range of δ 4.86-2.50 ppm and also support the corresponding ratio of THF molecules per carboranyl for all compounds. In addition, their solid state IR spectra display bands in the range 2300-2500 cm^{-1} characteristic of B-H···M interactions.

The polymeric structure of all complexes **(69)-(73)** was confirmed by single-crystal X-ray analysis. All compounds adopt a polymeric arrangement in which the metal atom (Na or K) and the 12 vertexes *nido*-carborane ligand serve as alternating linkages to give a zigzag infinite chain that is maintained in one dimension throughout the lattice. In the case of (**69**)[44] (Figure 12) each asymmetric unit consists of two [{μ-1,2-[*o*-C_6H_4(CH_2)$_2$]-1,2-$C_2B_{10}H_{10}$}{$Na_2(THF)_3$}] structural motifs that are related to each other by an inversion center. One Na^+ is η^6-bound to the open six-member C_2B_4 face and coordinated to one THF molecule and one neighbouring 'carbons-adjacent' *nido*-carborane via two B-H···Na bonds. The second Na^+ is bonded to a trigonal B_3 face through three B-H···Na bonds and to the neighboring 'carbons-adjacent' *nido*-carborane via two B-H···Na bonds and coordinated to two THF molecules. The average Na(1)-cage atom and Na(2)···B(H) distances are of 2.854(4) and 3.026(4)Å, respectively.

The most significant part of the structure of polymer **(70)**[44] (Figure 13) is the monoanion [$R_2C_2B_{10}H_{11}]^-$, which was first observed experimentally. This ligand

possesses two pentagonal belts: a C_2B_3 that is partially capped by one μ_3-H atom (Chart 7b) and one B_5 that is capped by the remained two boron atoms.

Polymer **(71)**[44] (Figure 14) shows the novel [*nido*-μ-1,4-$R_2C_2B_{10}H_{10}$]$^{2-}$ dianion (Chart 7c), which has a basket structure with a highly distorted six-membered C_2B_4 ring. The average C_c-C-C_{aryl} angle of 109.7(2)° and the dihedral angle between the two aromatic rings of 68.9º in **71** are much smaller than in its parent *closo* μ-1,2-[1,1'-$(C_6H_4)_2$-2,2'-$(CH_2)_2$]-1,2-$C_2B_{10}H_{10}$ molecule, 117.8(3)º and 66.1º, respectively.

On the other hand, polymers **72** and **73** show a similar zigzag carborane-Na-carborane-Na infinite chain but a different dianionic *nido*-carborane cage (Chart 7d,e).[45] The [*nido*-1,3-$(CH_2)_5$-1,3-$C_2B_{10}H_{10}$]$^{2-}$ ligand in polymer **72** (Figure 15) represents a new member of the 12-vertexes *nido* clusters family, in which two connectivities, C_c-C_c and C_c-B(3), are broken during the reductive process leading to the formation of a highly distorted five-member C_2B_3 face with an elongated C(1)-B(3) bond (Chart 7d). In polymer [{1,4-$(CH_2)_6$-1,4-$C_2B_{10}H_{10}$}{$Na_2(THF)_4$}]$_n$ **(73)** as the linkage size increases by one methylene unit, the C(1)-B(3) distance is forced to be further separated, generating a highly distorted six-membered C_2B_4 face (Chart 7e). The structural parameters of the *nido*-carborane cage in **73** are close to these observed in polymer **71.**[44] These data suggest that the overall ring forces of the $(CH_2)_6$ and 1,1'-$(C_6H_4)_2$-2,2'-$(CH_2)_2$ links acting on the cage are similar, although the rigidity of the bridges is quite different. These results show that although both the bridge length and the rigidity of C,C'-linked *o*-carboranes have significant effects on the formation of carborane anions, the former plays a more important role than the latter in controlling the relative positions of the two cage carbon atoms during the reductive process.[45]

The first structurally characterized example of a metallacarborane of K^+ corresponds to the polymer [*closo-exo*-{$(C_6H_5CH_2)_2C_2B_{10}H_{10}$}$K_2(THF)_2(O_2C_4H_8)0.5$]$_n$ **(74)** [46] that

adopts a structure in which the dioxane and the potassium ion serve as alternating bridging groups to give a zigzag chain (Figure 16). One K^+ ion is η^6-bonded to the hexagonal C_2B_4 face of the cage forming a 13-vertex metallacarborane structural motif (Chart 7f) that is also coordinated to one oxygen atom of the bridging dioxane molecule. The other K^+ ion is bonded to two trigonal B_3 faces through two sets of three unequal B-H···K bonds from two neighboring carborane cages; its coordinating sphere is completed by two THF molecules.

In general, metallocarboranes of the heavier Group 2 metals are fewer in number; the only structurally characterized example of a polymeric metallocarborane of Group 2 salts corresponds to the compound [*closo*-1,1,1-$(MeCN)_3$-1,2,4-$Sr(C_2B_{10}H_{12})]_n$ **(75)** (Figure 17).4 The structure shows a spiral-chain whose units are linked by inter-cage Sr-H-B and Sr-H-C. Each carborane fragment (Chart 7g) serves as a ligand to two Sr atoms, bonded to one through an open hexagonal face and to the other via upper- and lower- belt E-H···M (E= B or C) interactions. The coordination geometry about each Sr is completed by three CH_3CN ligands. It is noteworthy that one of the C-H vertexes of each carborane fragment interacts with the Sr. A more detailed view of the metal to the carborane interaction can be seen in Figure 17.

Polymeric structures of the heavier Group 14 elements, Sn and Pb, with carborane were prepared by chloride ion abstraction from $[SnEt_3]Cl$ and $[PbEt_3]Cl$, respectively, using the halogenated carborane anion $[CB_{11}H_6Br_6]^-$.[47] Crystal structures $[Et_3E(CB_{11}H_6Br_6)]_n$ (E= Sn **(76)** or Pb **(77)**) adopt five-coordinate trigonal-bipyramidal geometries. The carborane anions are bridging axial ligands connecting trigonal $[EEt_3]^+$ cation-like moieties in the polymeric chain structures, through Br atoms of the $[CB_{11}H_6Br_6]^-$ unit (Figure 18).

2.- Polymers with d-block elements.

The treatment of $[NMe_4][1,1'\text{-}(PPh_2)_2\text{-}3,3'\text{-}Co(1,2\text{-}C_2B_9H_{10})_2]$ with one equivalent of $AgClO_4$ in ethanol/acetone leads to 1D-coordination polymer $[Ag\{1,1'\text{-}(PPh_2)_2\text{-}3,3'\text{-}Co(1,2\text{-}C_2B_9H_{10})_2\}(OCMe_2)]_n$, **(78)** (Figure 19).[48] The silver cation is tetrahedrally coordinated by two P atoms from the carborane, one O atom from the acetone ligand and one neighboring *closo*-carborane via one B-H···Ag. The H···Ag distance of 2.17Å is shorter than distances observed in other silver polymers containing the (**1**) anion.[43]

The incorporation of carborane clusters as linkers in coordination polymers can be realized by introducing the metal-binding group directly bonded to the cage. Carboranylcarboxylate ligands have been used to introduce C_2B_{10}-cages into the backbone of 1D coordination polymers. The reaction of two different carboranylcarboxylate ligands, 1-R-2-CO_2H-1,2-*closo*-$C_2B_{10}H_{10}$ (R= CH_3, H**)** with $MnCO_3$ in water leads to the polymeric compounds $[Mn(\mu\text{-}H_2O)(\mu\text{-}1\text{-}CH_3\text{-}2\text{-}CO_2\text{-}1,2\text{-}closo\text{-}C_2B_{10}H_{10})_2]_n\cdot(H_2O)_n$ **(79)**[49] or $[Mn(H_2O)(\mu\text{-}1\text{-}CO_2\text{-}1,2\text{-}closo\text{-}C_2B_{10}H_{11})_2]_n\cdot 2H_2O$ **(80)**,[50] respectively. X-ray analysis (Figure 20 a,b) revealed substantial differences between both compounds attributed to the existence of different substituents, -CH_3 or -H, on one of the C_c of the carboranylcarboxylate ligand. While a six-coordinated Mn^{II} compound with water molecules bridging each two Mn^{II} centers was observed in **(79)**, a square pyramidal geometry around each Mn^{II} ion with terminal water molecules coordinated to each Mn^{II} center was found **(80)**. The structures of these polymers display an unusual feature among the 1D oligomer Mn^{II} complexes with a nuclearity higher than two, that is, the existence of water molecules bridging two Mn centers or the existence of terminal water molecules, depending on the carboranylcarboxylate ligand used.

The packing structure of polymer **(79)** displays polymeric chiral chains with two different conformations (Δ and Λ) due to the orientation of the CH_3 groups from the

carboranylcarboxylate ligands (Figure 21). The orientation of the CH_3 groups is the same within a chain and opposite to the CH_3 groups from a different chain. However, the polymeric chiral chains displayed in **(79)** are not observed in **(80)**.

The polymeric nature of both compounds can be easily fragmented by coordinating solvents, e.g. diethyl ether, generating oligomer species. Moreover, the reactivity of polymer **(79)** with Lewis bases as 2,2'-bipyrimidine, leads to the formation of a new hybrid polymer $[Mn(1\text{-}CH_3\text{-}2\text{-}CO_2\text{-}1,2\text{-}\textit{closo}\text{-}C_2B_{10}H_{10})_2(bpm)]_n$ **(81)** (Figure 22). Magnetic measurements show weak antiferromagnetic interactions between the Mn atoms in all cases.

3.- Polymers with f-block elements.

The reaction of $[Me_2Si(C_9H_5C_2H_2OMe)(C_2B_{10}H_{10})]Li_2(OEt_2)_2$ with an equimolar amount of SmI_2 in THF results in the isolation of the polymer $[\{[\eta^5{:}\sigma\text{-}Me_2Si(C_9H_5CH_2CH_2OMe)(C_2B_{10}H_{10})]_2Sm\}\{Li(THF)\}]_n$ **(82)**.[51] Compound **(82)** is a coordination polymer with Li(THF) as a linkage connecting two anionic $[\{[\eta^5{:}\sigma\text{-}Me_2Si(C_9H_5CH_2CH_2\text{-}OMe)(C_2B_{10}H_{10})\}_2Sm]^-$ fragments via the tethered oxygen atoms (Figure 23). The formation of **(82)** results from the Sm(II) electron transfer to the cluster. It may be suggested that the reaction of $SmI_2(THF)x$ with $[Me_2Si(C_9H_5C_2H_2OMe)(C_2B_{10}H_{10})]Li_2(OEt_2)_2$ gives the first intermediate $[\eta^5{:}\eta^1{:}\sigma\text{-}Me_2Si(C_9H_5CH_2\text{-}CH_2OMe)(C_2B_{10}H_{10})]Sm^{II}$, followed by intermolecular electron transfer and then ligand redistribution to afford polymer **(82).**

The reaction of $EuI_2(THF)_2$ with equimolar amounts of $Na_2[\textit{nido}\text{-}C_2B_{10}H_{12}]$ in THF results in the isolation of half-sandwich lanthanacarborane $[(\eta^6\text{-}C_2B_{10}H_{12})Eu(THF)_3]_n$ that after recrystallization from $MeCN/Et_2O$ gives a MeCN coordinated species $[(\eta^6\text{-}C_2B_{10}H_{12})Eu(MeCN)_3]_n$ **(83)** (Figure 24).[52] Single-crystal X-ray analyses shows a spiral chain where each carborane moiety serves as a ligand for two europium atoms, and each

Eu^{2+} ion is η^6-bonded to one $C_2B_{10}H_{12}^{2-}$ ligand and σ-bonded to three MeCN molecules and two E-H (E=/cage B and C atoms) bonds from the neighboring carboranyl ligand in a highly distorted-octahedral geometry. The fragment C_2B_{10} in this compound can be compared with the previously described Sr metallocarborane polymer **(75).**

The reaction of $Me_2Si(C_9H_7)(C_2B_{10}H_{11})$ with excess of NaH followed by Na metal afforded $[\{Me_2Si(C_9H_7)(C_2B_{10}H_{11})\}\{Na_3(THF)_n\}]$ that reacts with $ErCl_3$ in THF leading to $[\{\eta^5:\eta^6\text{-}Me_2Si(C_9H_6)(C_2B_{10}H_{11})\}Er(THF)(\mu\text{-}Cl)Na(THF)_2]_n$[53] **(84)** (Figure 25) after recrystallization from toluene/THF. This complex shows a polymeric chain where the Er^{3+} ion is η^5-bound to the indenyl group, η^6-bound to the hexagonal C_2B_4 face of the *nido*-carborane cage, σ-bound to one bridging chlorine atom and coordinated to one THF molecule in a distorted-tetrahedral arrangement. The cation $[Na(THF)_2]^+$ acts as a linkage to connect two $[\{\eta^5:\eta^6\text{-}Me_2Si(C_9H_6)(C_2B_{10}H_{11})\}Er(THF)(\mu\text{-}Cl)]^-$ fragments.

closo 1,2-$C_2B_{10}H_{12}$ can undergo four-electron reduction with excess alkali metals in the presence of f-block lanthanide metal halides to form a *arachno* $[C_2B_{10}H_{12}]^{4-}$ tetraanion. This 12 vertexes *arachno* cluster is capable of being η^7-bound to metal ions leading to 13-vertex *closo*-metallacarboranes, which can be obtained also through the *nido*-carborane lanthanide metals. Chart 8 shows different 12 vertexes *arachno* carboranyl ligands involved in the coordination polymers (**85**) - (**91**).

The reaction of $[\{\eta^5\text{-}Me_2C(C_5H_4)(C_2B_{10}H_{11})\}\{ErCl_2(THF)_3\}]$ or $[\{\eta^5:\eta^6\text{-}Me_2C(C_5H_4)(C_2B_{10}H_{11})\}\{Er(THF)_2\}]$ with excess Na metal in THF at room temperature affords the same $[\{[\eta^5:\eta^7\text{-}Me_2C(C_5H_4)(C_2B_{10}H_{11})]Er\}_2\{Na_4(THF)_9\}]_n$ **(85)** compound.[54] The polymeric nature of **(85)** confirmed by X-ray diffraction indicates that each asymmetrical unit contains two $[\eta^5:\eta^7\text{-}Me_2C(C_5H_4)(C_2B_{10}H_{11})Er]^{2-}$ structural motifs that are connected by three Na atoms through several B-H···Na three-center-two-electron bonds (3c-2e). The asymmetrical units are linked to each other via B-H···Er

bonds to form the polymeric chain. Each metal ion is η^7-bound to the *arachno*-carboranyl ligand (Chart 8a), η^5-bound to the cyclopentadienyl and σ-bound to two B-H bonds from the neighboring *arachno*-carboranyl unit in a distorted tetrahedral arrangement.

The *nido* carborane in polymer **(84)** can accept two electrons from sodium to become the *arachno* species resulting in the isolation of polymer **(86)** $[\{\eta^5{:}\eta^7\text{-}[Me_2Si(C_9H_6)(C_2B_{10}H_{11})]Er\}_2\{Na_4(THF)_8\}]_n$,[53] which asymmetrical unit contains two $[\eta^5{:}\eta^7\text{-}Me_2C(C_9H_6)(C_2B_{10}\text{-}H_{11})]Er^{2-}$ synthons that are linked via B-H···Na bonds forming a polymeric chain (Figure 26). The same polymer containing Dy, $[Me_2Si(C_9H_6)(C_2B_{10}H_{11})]Dy\}_2\{Na_4(THF)_8\}]_n$ **(87)** (Figure 27), is obtained by reaction of $Me_2Si(C_9H_7)(C_2B_{10}H_{11})$ with excess of NaH in THF followed by addition of $DyCl_3$ in excess of Na.[53] The two infinite polymeric chains are isostructural and isomorphous. X-ray analyses reveal a similar structure between these polymers and the polymer **(85).**[54] The average Ln-C(C_5 ring), Ln-C(cage) and Ln-B(cage) distances in (**86)** and **(87**) are longer than the corresponding values found in its cyclopentadienyl analogue of $[\{[\eta^5{:}\eta^7\text{-}Me_2C(C_5H_4)(C_2B_{10}H_{11})]Er\}_2\{Na_4(THF)_9\}]_n$ **(85).**[54]

These results indicate that the substituents indenyl or cyclopentadienyl, on carborane cage carbons may affect the overall molecular structures of the 13-vertex *closo*-metallacarborane complexes, but have little influence on the interactions between the central metal ion and the *nido*- or *arachno*-carborane ligand.

The presence of other substituents on the carborane ligands as $Me_2NCH_2CH_2$- and $MeOCH_2CH_2$- leads to the isolation of a new class of 13-vertex *closo*-metallacarboranes.[55] Treatment of 1-($Me_2NCH_2CH_2$)-1,2-$C_2B_{10}H_{11}$ with excess of Na in THF, followed by reaction with 1 equiv of YCl_3 afforded the polymeric compound $[\{\eta^1{:}\eta^7\text{-}[(Me_2NCH_2CH_2)C_2B_{10}H_{11}]Y(THF)\}\{Na(THF)_2\}]_n$ **(88)**, (Figure 28). A similar

synthetic process using 1,2-$(Me_2NCH_2CH_2)_2$-1,2-$C_2B_{10}H_{10}$ or 1-$Me_2NCH_2CH_2$-2-$MeOCH_2CH_2$-1,2-$C_2B_{10}H_{10}$ with $LnCl_3$, (Ln=Y, Eu) leads to the formation of $[\{\eta^1:\eta^1:\eta^7$-$[(Me_2NCH_2CH_2)_2C_2B_{10}H_{10}]Y\}\{Na(MeCN)_2\}]_n$, **(89)**, $[\{\eta^1:\eta^1:\eta^7$-$[(Me_2NCH_2CH_2)(MeOCH_2CH_2)C_2B_{10}H_{10}]Y\}\{Na(MeCN)\}]_n$ **(90)** or $[\{\eta^1:\eta^1:\eta^7$-$[(Me_2NCH_2CH_2)(MeOCH_2$-$CH_2)C_2B_{10}H_{10}]Er\}\{Na(MeCN)(THF)\}]_n$ **(91)** after recrystallization from MeCN/toluene/THF. In all compounds, each rare earth metal ion is η^7-bound to the *arachno*-carboranyl ligand and σ-bound to two B-H vertexes from the open face of the neighboring *arachno*-carboranyl cage, and coordinated to one nitrogen atom of the pendant amido substituent and one THF solvent molecule in **(88)** (Figure 28) whereas in compounds **(89-91)** one DCH_2CH_2 moiety (D= Me_2N or MeO) is replacing one THF molecule (Figure 29). These results show that the coordination of the second side arm, either Me_2N or MeO, does not largely alter the basic structural unit and the overall coordination environments around the lanthanide ions. The lower number of solvent molecules around the Na, less than three, probably leads to the formation of polymeric chains.

VI. Conclusions and outlook

The incorporation of icosahedral boron clusters to π-conjugated polymers improves their stability and solubility and clearly alters their electrochemical, photoluminescent and electrochromic properties. The PPy films doped with anionic boron clusters act as a cation exchanger with the media therefore is an excellent candidate for the implementation of selective ion exchange resins controlled by an electrochemical potential. Further, metallacarborane doping agents produce the highest ORL on these materials. Among them, the self-doped PPy films produce an electrical material that even after having lost its electroactivity caused by a high destabilizing potential recovers the electroactivity in few hours. Icosahedral boron clusters-containing silane,

siloxane-acetylene, polyaryl(ether), polyimides possess exceptional thermal, thermo-oxidative, and elastic properties making them excellent candidates for high-temperature elastomers. After pyrolysis at very high temperatures, these polymers form high thermally stable ceramics that resist oxidative degradation. Icosahedral carboranyl C_2B_{10} ligands are capable of producing fascinating motifs of coordination to metals η^7-, η^6-, η^5- and σ-, which makes them attractive for new types of unconventional coordination chemistry. In addition, icosahedral boron clusters induce unconventional properties in the supramolecular structures in which they are inserted due to the possibility to produce hydrogen and dihydrogen bonding.

The reported results on these hybrid π conjugated polymers presumes that boron clusters will be intervening parts in the development of organic electronics particularly on technological applications such as organic photovoltaics (OPVs), organic light-emitting diodes (OLEDs), field effect transistors (FETs), sensors, and electrochromic devices. In addition, the flexible, plastic nature of the COPs materials used in electronic devices has led to the realistic promise of flexible electronics in the near future. Silane and siloxane carboranyl containing polymers are promising precursors for flame retardant materials, with particular attention to paper products as a way to find application for forest, nowadays that the electronic books are taking a dominant role.

The particular properties of boron cluster ligands may induce unconventional properties to coordination polymers' structures making them useful for gas storage and separation, energy conversion, catalysis, bio-medical, molecular recognition and magnetic and luminescent materials.

CHARTS CAPTION

Chart 1.- Icosahedral heteroboranes with their vertex numbering: *closo* $[B_{12}H_{12}]^{2-}$, *closo* $[CB_{11}H_{12}]^{-}$, *nido* $[C_2B_9H_{12}]^{-}$, isomers of *closo* $C_2B_{10}H_{12}$ carboranes (*ortho*- (1,2), *meta*- (1,7), and *para*- (1,12)) and metallacarboranes $[3,3'\text{-}M(1,2\text{-}C_2B_9H_{11})_2]^{-}$, M= Co(III) in (**1**) and M= Fe(III) in (**2**). Pink circles correspond to B-H vertexes while the grey circles to C-H vertexes.

Chart 2.- Pyrrole, thiophene and dioxithiophene monomers and the pentagonal cycle vertexes numbering.

Chart 3.- Chemical structures of the $[B_{12}H_{12}]^{2-}$ (**3**) and its derivatives (**4**)-(**8**). White circles correspond to B-H while the dark circles to B-I vertexes and the grey circles to a B atom.

Chart 4.- Chemical structures of the anionic metallabisdicarbollides (**1**) and (**2**) and its derivatives (**9**)-(**18**). White circles vertexes correspond to B-H while the dark circles to C_c-H vertexes and grey circle to B atom.

Chart 5.- Chemical structures of the monosubstituted (**19**) - (**22**) and disubstituted (**23**) and (**24**) neutral pyrroles, as well as the anionic (**25**) and (**26**) ones. Vertexes correspond to B-H while the circles to C_c atom.

Chart 6.- Chemical structures of the monosubstituted neutral (**27**), (**28**), (**30**)-(**33**), (**34**) and anionic (**29**), (**33**), (**35**) and (**36**) thiophenes. Vertexes correspond to B-H while the circles to C_c atom.

Chart 7. View of the different positional 12 vertexes *nido* carboranyl ligands involved in the coordination polymers (**76**)-(**82**). Vertexes correspond to B-H while the dark circles to C_c atom.

Chart 8. View of the different 12 vertexes *arachno* carboranyl ligands involved in the coordination polymers (**92**)-(**98**). Vertexes correspond to B-H while the circles to C_c atom.

Chart 1.- Icosahedral heteroboranes with their vertex numbering: *closo* $[B_{12}H_{12}]^{2-}$, *closo* $[CB_{11}H_{12}]^{-}$, *nido* $[C_2B_9H_{12}]^{-}$, isomers of *closo* $C_2B_{10}H_{12}$ carboranes (*ortho*- (1,2), *meta*- (1,7), and *para*- (1,12)) and metallacarboranes $[3,3'\text{-}M(1,2\text{-}C_2B_9H_{11})_2]^{-}$, M= Co(III) in (**1**) and M= Fe(III) in (**2**). Pink circles correspond to B-H vertexes while the grey circles to C-H vertexes.

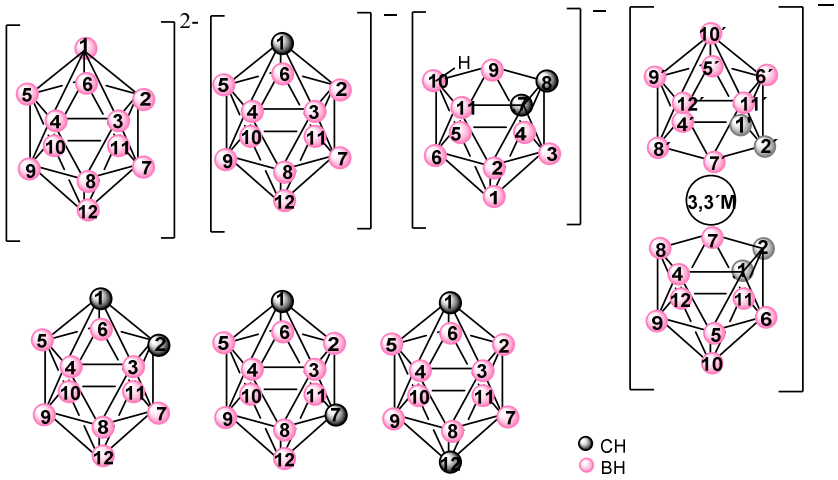

Chart 2.- Pyrrole, thiophene and dioxithiophene monomers and the pentagonal cycle vertexes numbering.

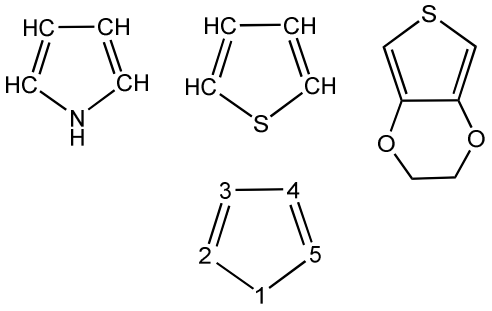

Chart 3.- Chemical structures of the $[B_{12}H_{12}]^{2-}$ (**3**) and its derivatives (**4**)-(**8**). White circles correspond to B-H while the dark circles to B-I vertexes and the grey circles to a B atom.

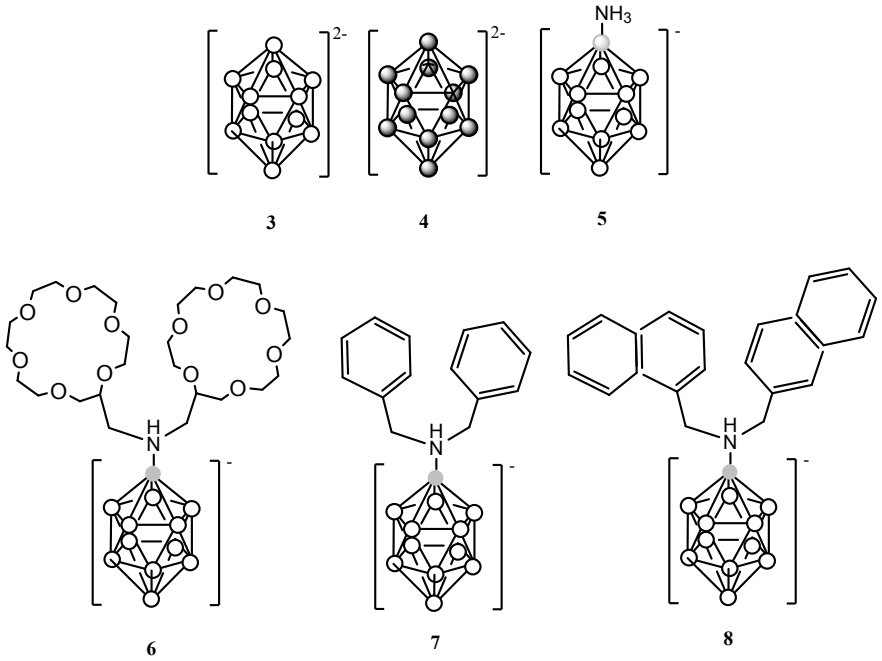

Chart 4.- Chemical structures of the anionic metallabisdicarbollides (**1**) and (**2**) and its derivatives (**9**)-(**18**). White circles correspond to B-H while the dark circles to C_c-H vertexes and grey circle to B atom.

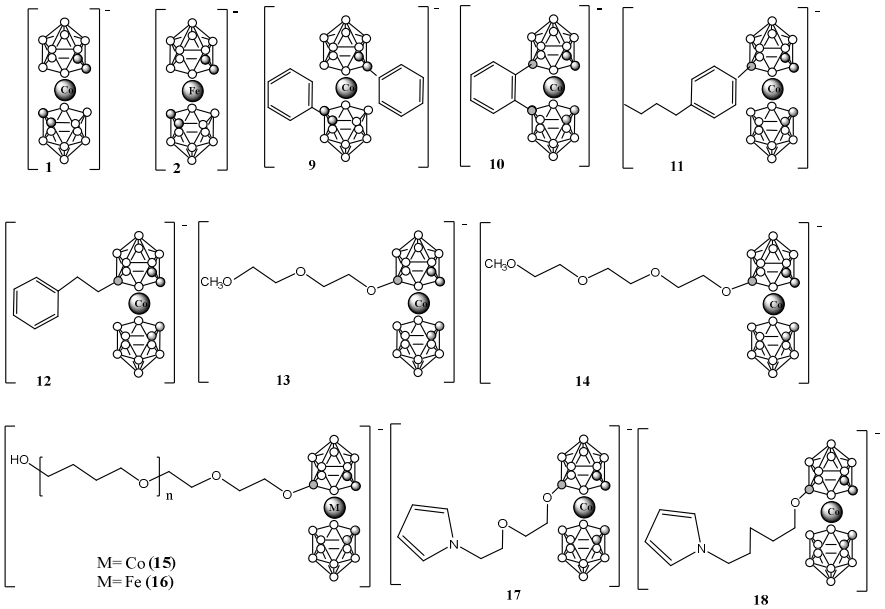

Chart 5.- Chemical structures of the monosubstituted (**19**) - (**22**) and disubstituted (**23**) and (**24**) neutral pyrroles, as well as the anionic (**25**) and (**26**) ones. Vertexes correspond to B-H while the circles to C_c atom.

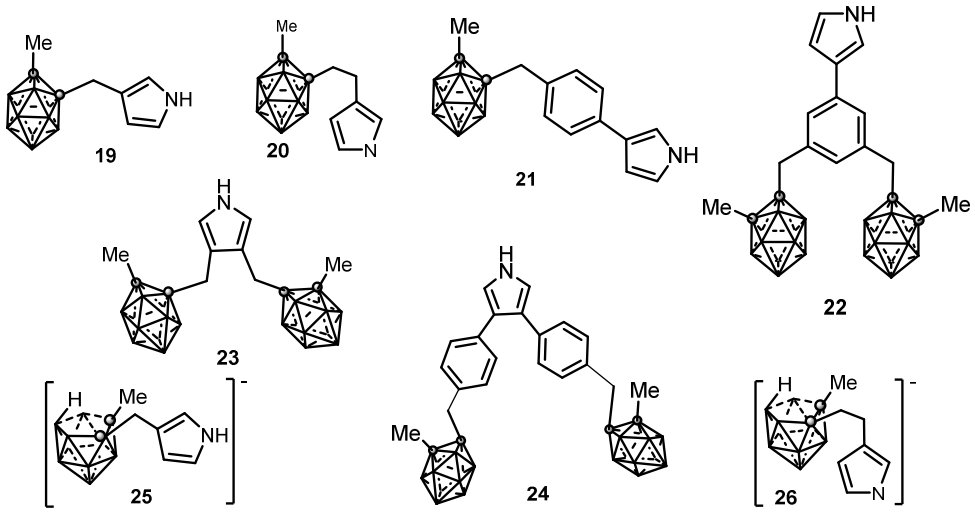

Chart 6.- Chemical structures of the monosubstituted neutral (**27**), (**28**), (**30**)-(**33**), (**34**) and anionic (**29**), (**33**), (**35**) and (**36**) thiophenes. Vertexes correspond to B-H while the circles to C_c atom.

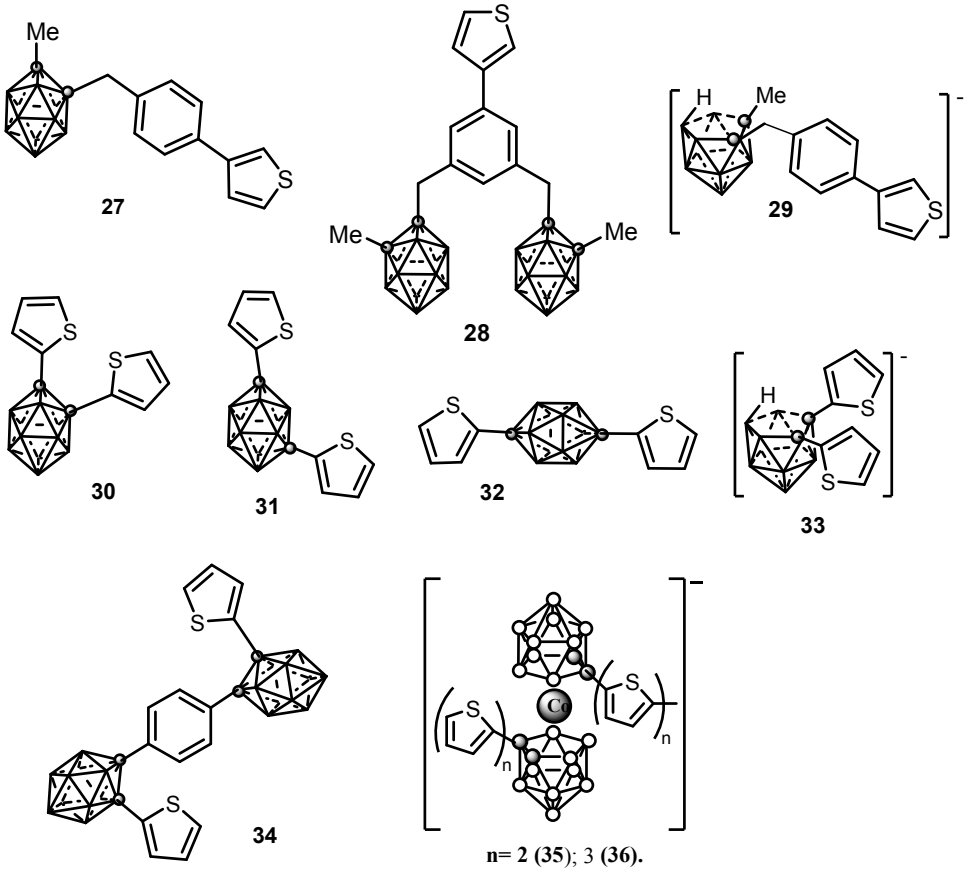

Chart 7. View of the different positional 12 vertexes *nido* carboranyl ligands involved in the coordination polymers (**69**)-(**75**). Vertexes correspond to B-H while the circles to C_c atom.

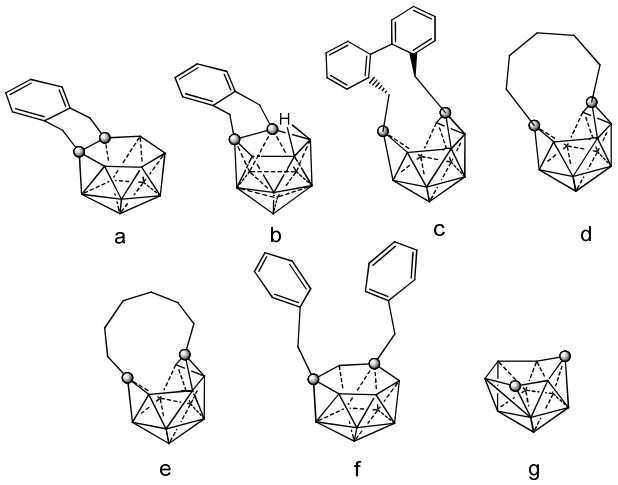

Chart 8. View of the different 12 vertexes *arachno* carboranyl ligands involved in the coordination polymers (**85**)-(**91**). Vertexes correspond to B-H while the circles to C_c atom.

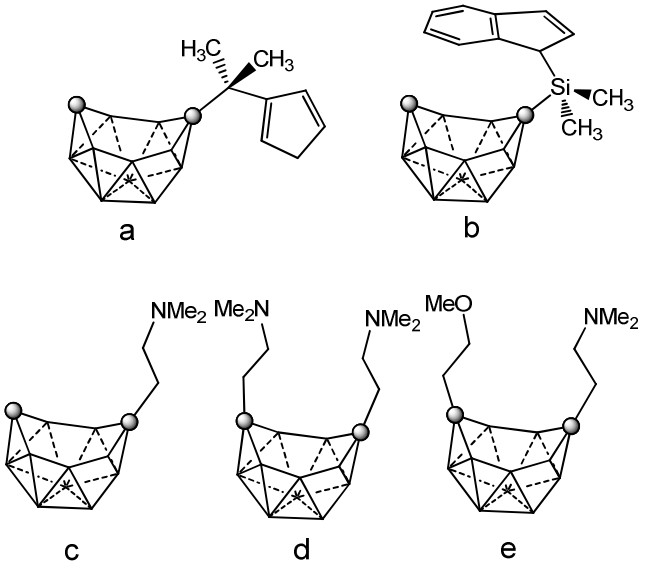

FIGURES CAPTION

Figure 1. Conducting and insulating states generated electrochemically. a) PPy; b) PTh.

Figure 2. a) Homogeneous and continuous intensity increases after each cycle. b) Pt electrode after growing during twenty cycles PPy with Cs(1) as doping agent.

Figure 3. Cyclic voltammetry of PPy(**1**) membranes in aqueous alkaline chlorides: LiCl 0.1 M; NaCl 0.1 M; KCl 0.1 M; RbCl 0.1 M; CsCl 0.1 M. Scan rate of electrode potential 20 mVs^{-1}.

Figure 4. Graphical representation of the PPy(**1**) polymer modified by $[NBu_4]^+$ and $[PBu_4]^+$.

Figure 5. Graphical representation of the PPy(**1**) polymer.

Figure 6. S.E.M. studies of PPy films doped with different anions: a) PPy($\mathbf{ClO_4}$); b) PPy(**DBS**); c) PPy(**1**) and its surface modification by $[NBu_4]^+$ and $[PBu_4]^+$, d) and e) respectively. (Figure 6d reproduced with permission from ref. 8. Copyright 2002, John Wiley and Sons)

Figure 7. a) LSV studies of PPy($\mathbf{PF_6}$), PPy($\mathbf{ClO_4}$), PPy(**1**) and copolymer PPy(**17**):PPy (1:4). LSV consists on the measurement of the current associated with overoxidation during a single scan (0 to 1.5 V *vs* Ag/AgCl) at low scan rate (0.5 mV/s) in a 0.5M KCl solution. b) Gradual self-repairing of copolymer PPy(**17**):PPy shown by ion exchange tests in NaCl 0.1 M: a) immediately after destabilizing the PPy(**17**):PPy by applying 1300 mV, b) after 30 minutes in the same electrolytic solution, c) after 1 h and d) after 18h.

Figure 8. a) XPS studies of PPy(**7**) membrane and b) XPS studies of overoxydized PPy(**7**) material. The membrane was set so that the side in contact with the solution is

the first to be sputtered. (Reproduced with permission from ref.10. Copyright 2005, Elsevier)

Figure 9. The different steps of the overoxidation process: a) doping anions migration; b) doping anions accumulation at the surface; c) doping anions expulsion due to its hydrophobic character. The zig-zag lines stand by the PPy chains while grey circles represent the positions of the doping anions and the empty circles the previously occupied position and the arrows indicate the trajectory of the moved anion. (Reproduced with permission from ref.10. Copyright 2005, Elsevier)

Figure 10. Proposed structures of the polymer PPy(**17**) and its copolymer (1:4) PPy(**17**):PPy.

Figure 11. Potentiodynamic curves obtained for a) polymerization of monomer (**17**). b) copolymerization of compound (**17**)with pyrrole (1:1). (Reproduced with permission from ref. 5. Copyright 2002, John Wiley and Sons)

Figure 12. 1D-polymer chain of **(69)**. H atoms omitted for clarity.

Figure 13. Molecular structure of **(70).** Some H atoms omitted for clarity.

Figure 14. Part of a 1D-chain in **(71)**. H atoms omitted for clarity.

Figure 15. Infinite polymer chain of **(72)**. H omitted by clarity.

Figure 16. a)Infinite polymer chain of **(74)**. H atoms omitted by clarity. b) View of the coordinating sphere around every K atom in **(74).**

Figure 17. Infinite polymer chain of **(75)**. (H atoms omitted by clarity) with a magnified view to visualize the metal to carboranyl ligand interactions.

Figure 18. a) Infinite polymeric chain of **(76)** and b) Closer view of the coordination environment in polymer **(77)** (H omitted for clarity).

Figure 19. Polymeric structure of **(78),** showing how the repetitive unit are connected to neighbouring molecules. H atoms omitted for clarity with the exception of B-H···Ag interactions.

Figure 20. Structure of polymers **(79)** and **(80)** showing the monodimensional arrangement. H atoms and water solvate omitted with the exception of the H substituent in **(80).**

Figure 21. X-ray structure of **(79)** showing different conformations for the polymeric chains. (Reproduced from Ref. 47 with permission from the Royal Society of Chemistry)

Figure 22. Infinite polymer chain of the hybrid $[Mn(1\text{-}CH_3\text{-}2\text{-}CO_2\text{-}1,2\text{-}\textit{closo}\text{-}C_2B_{10}H_{10})_2(bpm)]_n$ **(81)** (H atoms omitted by clarity).

Figure 23. Infinite polymer chain of **(82).** H atoms omitted for clarity.

Figure 24. Infinite polymer chain of **(83)** (H atoms omitted for clarity).

Figure 25. A portion of infinite polymer chain of **(84)** (H atoms omitted for clarity).

Figure 26. Molecular structure of $[\{\eta^5\text{:}\eta^7\text{-}[Me_2Si(C_9H_6)(C_2B_{10}H_{11})\}Er]_2^{4-}$ in **(86)**. H atoms omitted for clarity).

Figure 27. A portion of infinite polymer chain of **(87)**, (H atoms omitted for clarity).

Figure 28. A portion of the infinite polymeric chain of **(88)**. H atoms omitted for clarity.

Figure 29. A portion of the infinite polymeric chains of **(88-91)(a-d)**. H atoms omitted for clarity.

Figure 1. Conducting and insulating states generated electrochemically. a) PPy; b) PTh.

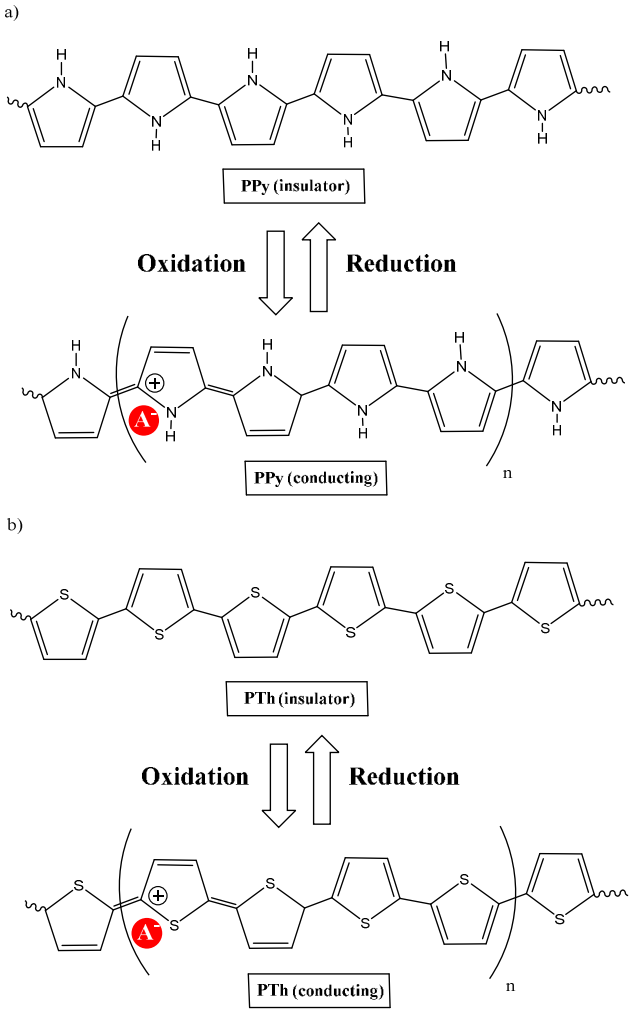

Figure 2. a) Homogeneous and continuous intensity increases after each cycle. b) Pt electrode after growing during twenty cycles PPy with Cs(1) as doping agent.

a) b)

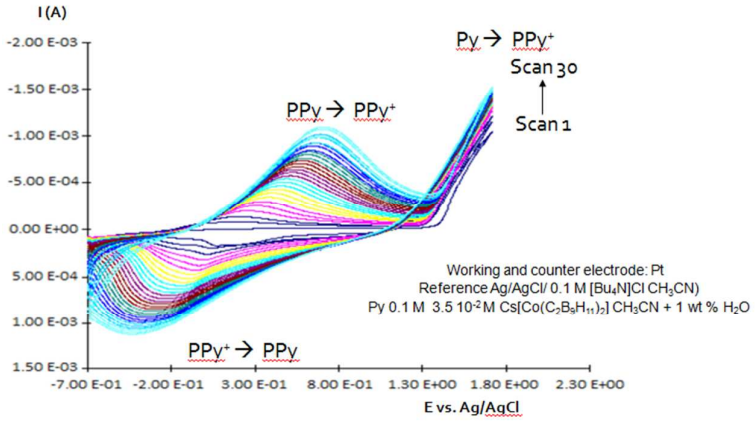

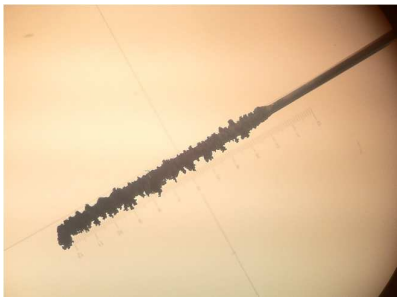

Figure 3. Cyclic voltammetry of PPy(**1**) membranes in aqueous alkaline chlorides: LiCl 0.1 M; NaCl 0.1 M; KCl 0.1 M; RbCl 0.1 M; CsCl 0.1 M. Scan rate of electrode potential 20 mVs^{-1}.

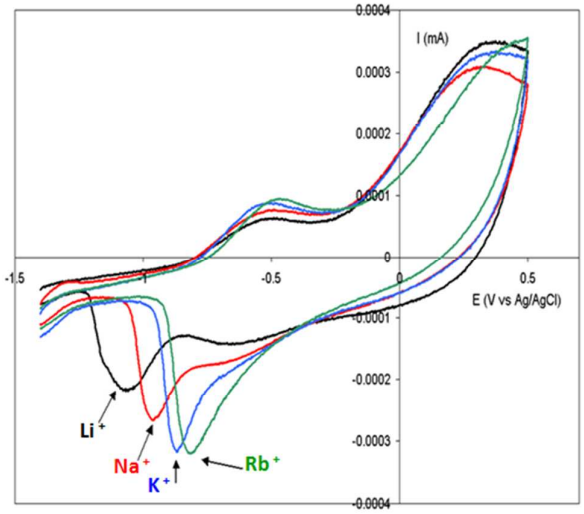

Figure 4. Graphical representation of the PPy(**1**) polymer modified by $[NBu_4]^+$ and $[PBu_4]^+$.

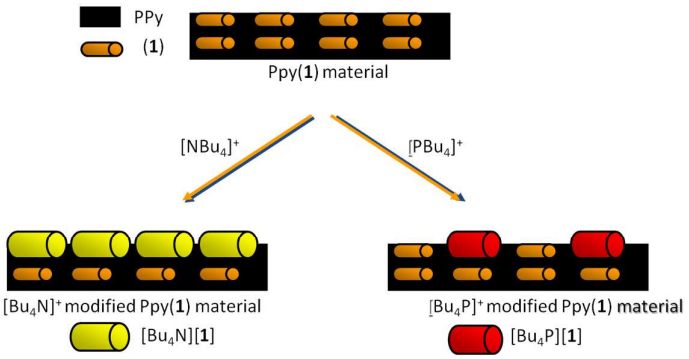

Figure 5. Graphical representation of the PPy(**1**) polymer.

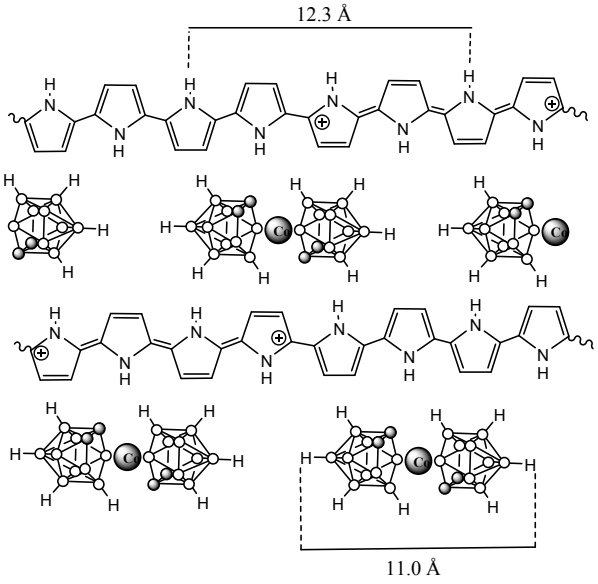

Figure 6. S.E.M. studies of PPy films doped with different anions: a) PPy(**ClO_4**); b) PPy(**DBS**); c) PPy(**1**) and its surface modification by $[NBu_4]^+$ and $[PBu_4]^+$, d) and e) respectively.

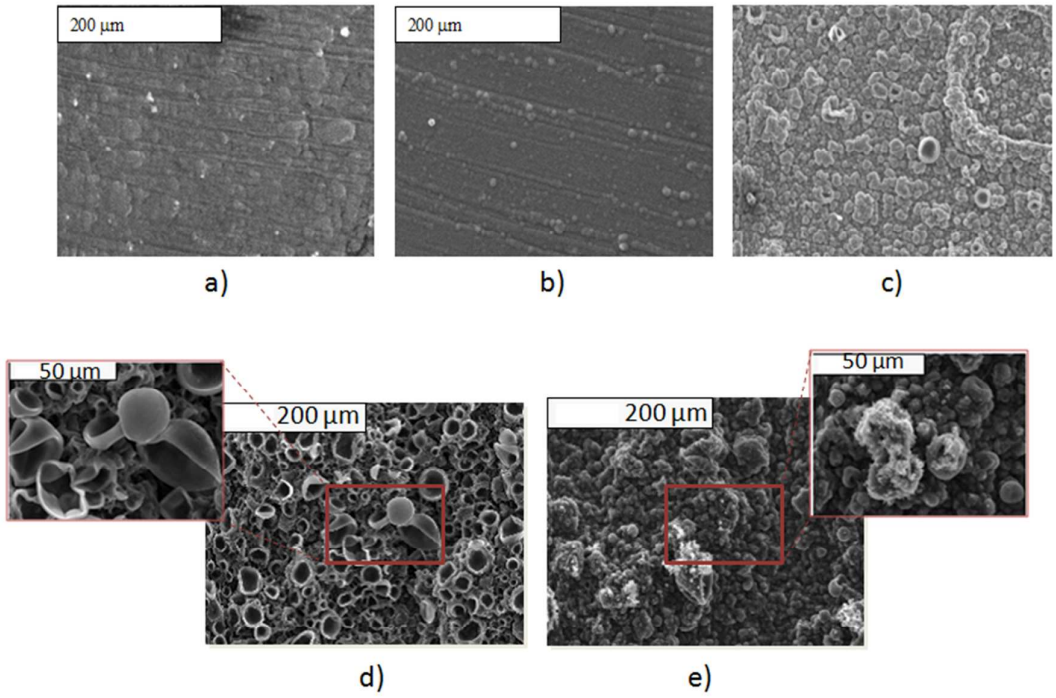

Figure 7. a) LSV studies of PPy(**PF_6**), PPy(**ClO_4**), PPy(**1**) and copolymer PPy(**17**):PPy (1:4). LSV consists on the measurement of the current associated with overoxidation during a single scan (0 to 1.5 V *vs* Ag/AgCl) at low scan rate (0.5 mV/s) in a 0.5M KCl solution. b) Gradual self-repairing of copolymer PPy(**17**):PPy shown by ion exchange tests in NaCl 0.1 M: a) immediately after destabilizing the PPy(**17**):PPy by applying 1300 mV, b) after 30 minutes in the same electrolytic solution, c) after 1 h and d) after 18h.

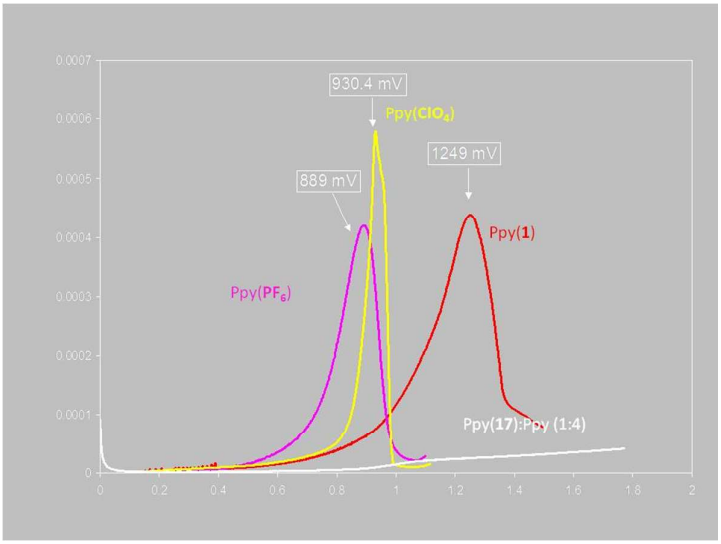

b)

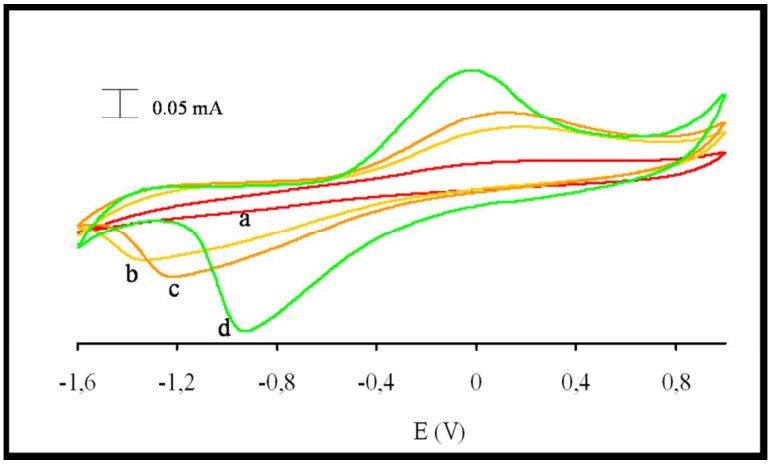

Figure 8. a) XPS studies of PPy(**7**) membrane and b) XPS studies of overoxydized PPy(**7**) material. The membrane was set so that the side in contact with the solution is the first to be sputtered.

a) b)

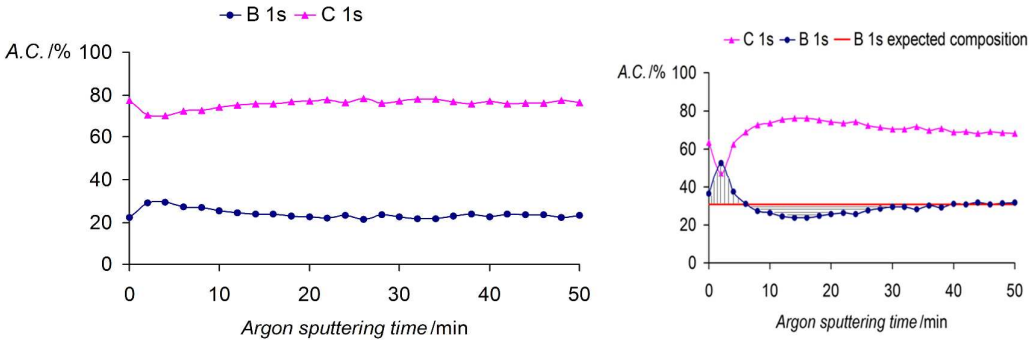

Figure 9. The different steps of the overoxidation process: a) doping anions migration; b) doping anions accumulation at the surface; c) doping anions expulsion due to its hydrophobic character. The zig-zag lines stand by the PPy chains while grey circles represent the positions of the doping anions and the empty circles the previously occupied position and the arrows indicate the trajectory of the moved anion.

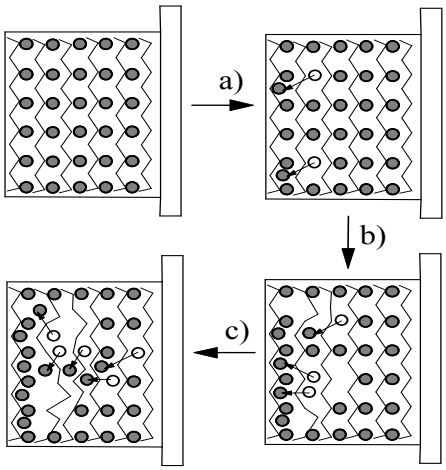

Figure 10. Proposed structures of the polymer PPy(**17**) and its copolymer (1:4) PPy(**17**):PPy.

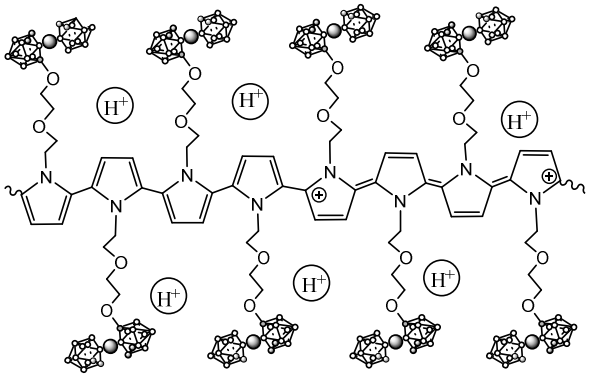

PPy(**17**)

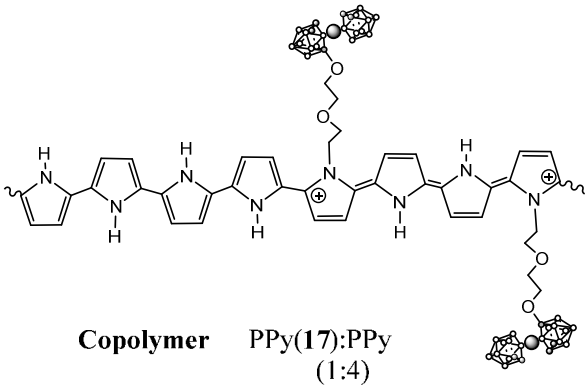

Copolymer PPy(**17**):PPy (1:4)

Figure 11. Potentiodynamic curves obtained for a) polymerization of monomer (**17**). b) copolymerization of compound (**17**)with pyrrole (1:1).

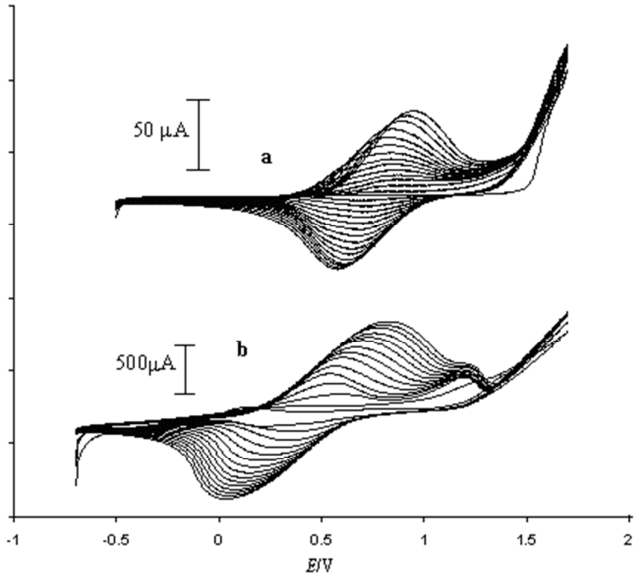

Figure 12. 1D-polymer chain of **(69)**. H atoms omitted for clarity.

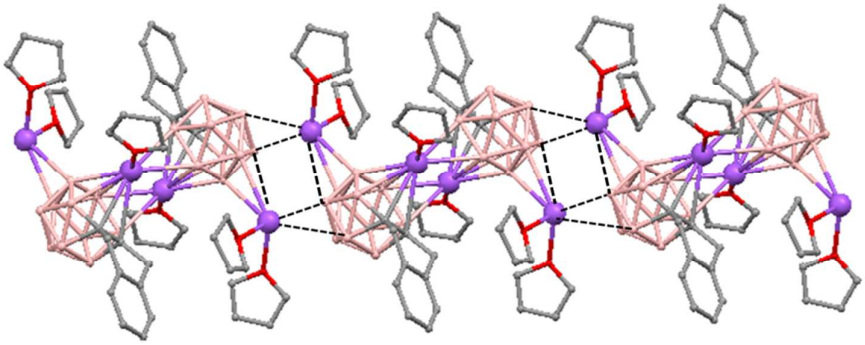

Figure 13. Molecular structure of **(70).** Some H atoms omitted for clarity.

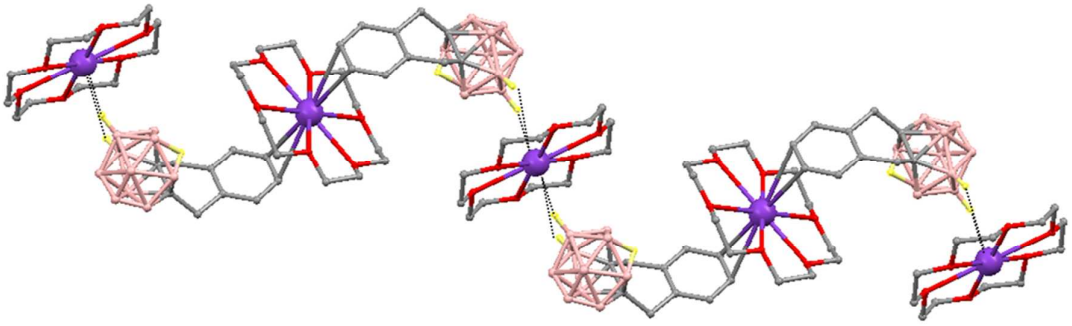

Figure 14. Part of a 1D-chain in **(71)**. H atoms omitted for clarity.

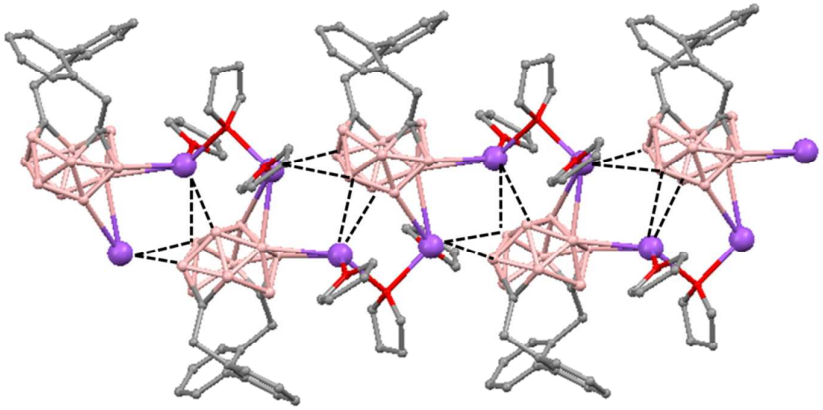

Figure 15. Infinite polymer chain of **(72)**. H omitted for clarity.

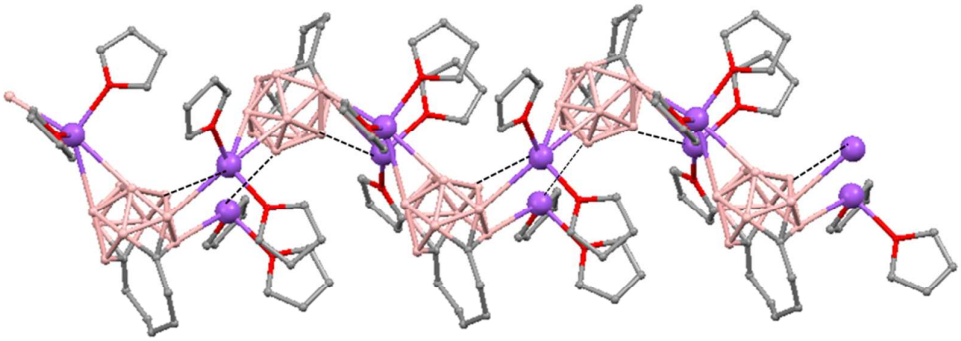

Figure 16. a)Infinite polymer chain of **(74)**. b) View of the coordinating sphere around every K atom in **(74).** H atoms omitted for clarity.

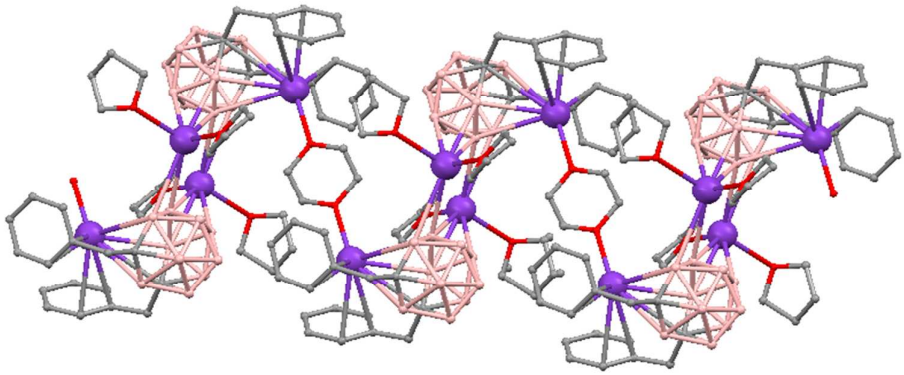

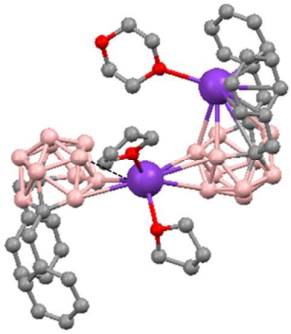

Figure 17. Infinite polymer chain of **(75)**. (H atoms omitted for clarity) with a magnified view to visualize the metal to carboranyl ligand interactions.

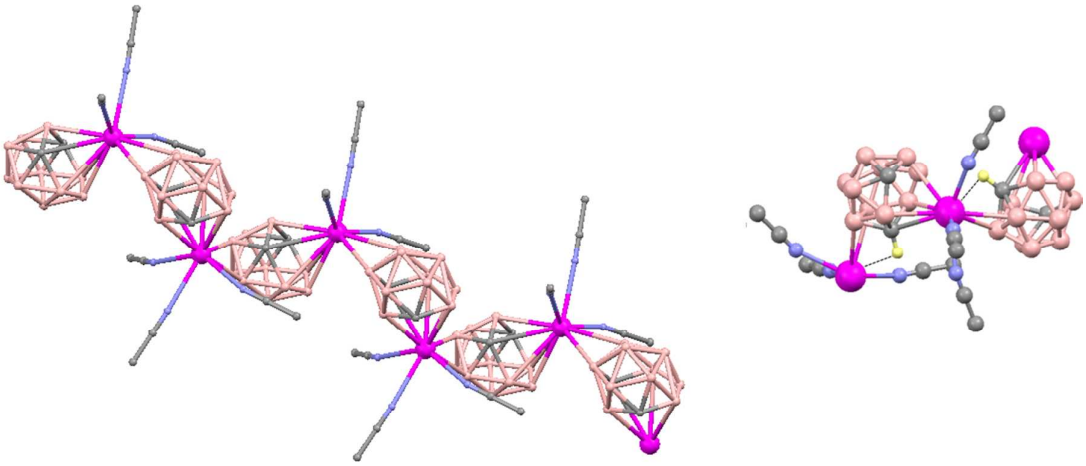

Figure 18. a) Infinite polymeric chain of **(76)** and b) Closer view of the coordination environment in polymer **(77)** (H omitted for clarity).

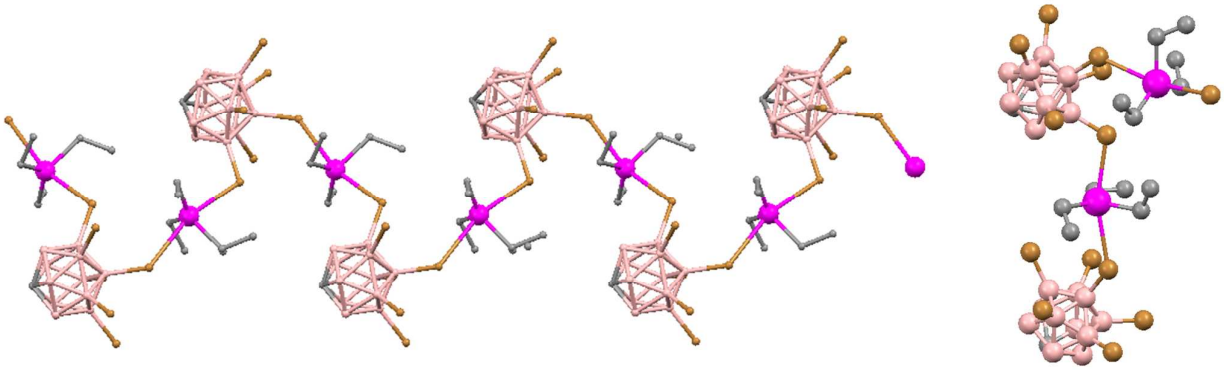

Figure 19. Polymeric structure of **(78),** showing how the repetitive units are connected to neighbouring molecules. H atoms omitted for clarity with the exception of B-H···Ag interactions.

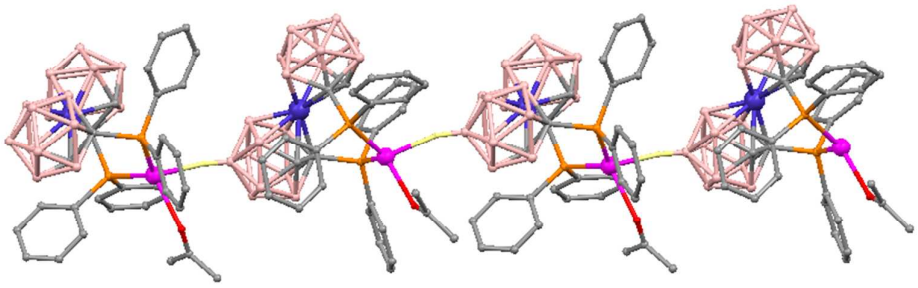

Figure 20. Structure of polymers **(79)** and **(80)** showing the monodimensional arrangement. H atoms and water solvate omitted with the exception of the H substituent in **(80).**

a) b)

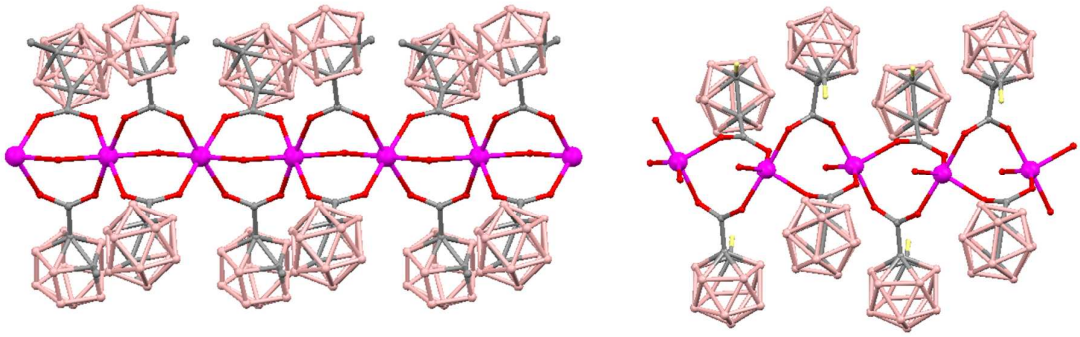

Figure 21. X-ray structure of **(79)** showing different conformations for the polymeric chains.

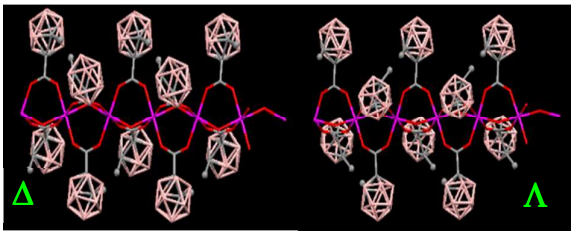

Figure 22. Infinite polymer chain of the hybrid $[Mn(1\text{-}CH_3\text{-}2\text{-}CO_2\text{-}1,2\text{-}\textit{closo}\text{-}C_2B_{10}H_{10})_2(bpm)]_n$ **(81)** (H atoms omitted for clarity).

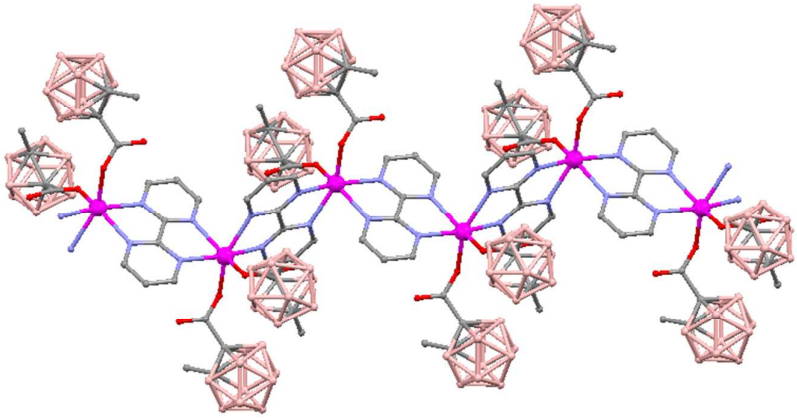

Figure 23. Infinite polymer chain of **(82).** H atoms omitted for clarity.

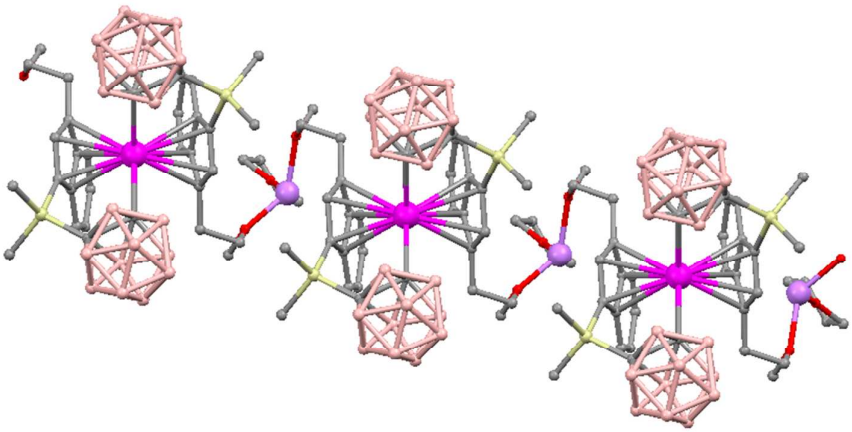

Figure 24. Infinite polymer chain of **(83)** (H atoms omitted for clarity).

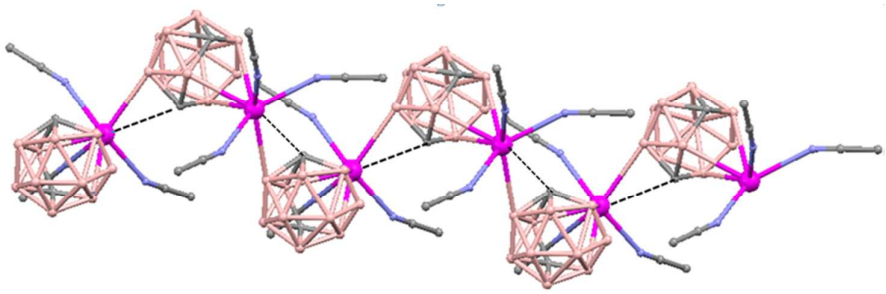

Figure 25. A portion of infinite polymer chain of **(84)** (H atoms omitted for clarity).

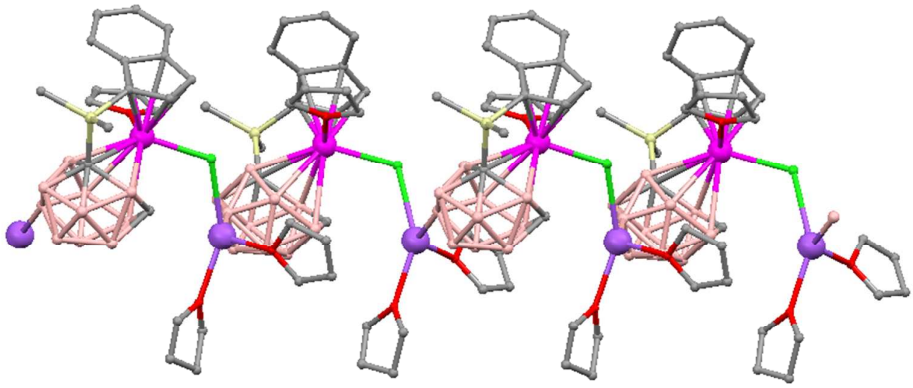

Figure 26. Molecular structure of $[\{\eta^5{:}\eta^7\text{-}[Me_2Si(C_9H_6)(C_2B_{10}H_{11})\}Er]_2^{4-}$ in **(86)**. H atoms omitted for clarity).

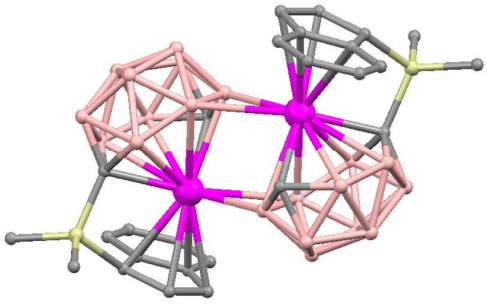

Figure 27. A portion of infinite polymer chain of **(87)**, (H atoms omitted for clarity).

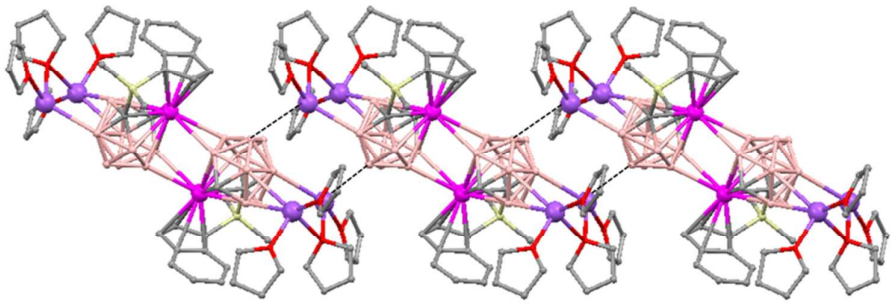

Figure 28. A portion of the infinite polymeric chain of **(88)**. H atoms omitted for clarity.

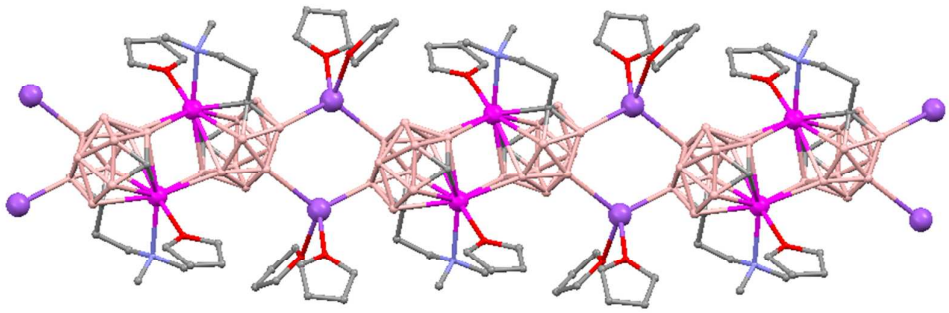

Figure 29. A portion of the infinite polymeric chains of **(88-91)(a-d)**. H atoms omitted for clarity.

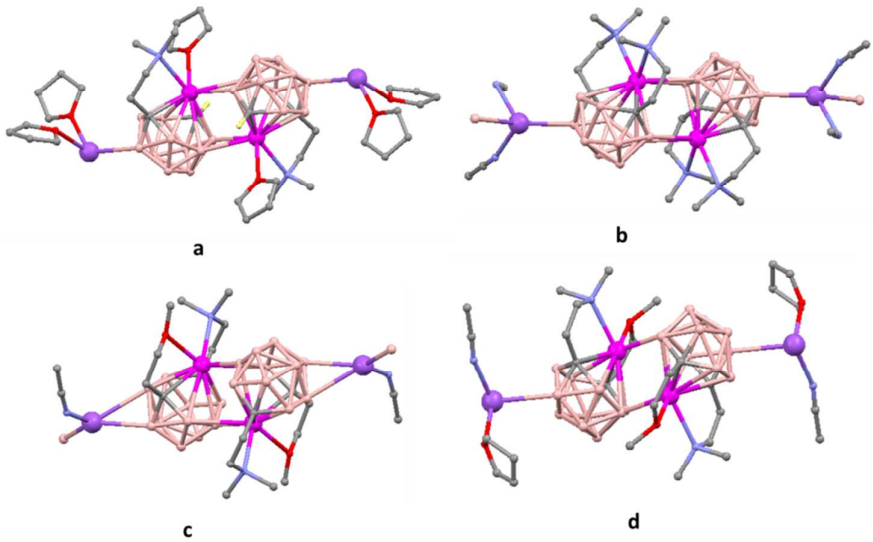

SCHEMES CAPTION

Scheme 1. The oxidation-reduction process in PPy(**1**) occurs via de-insertion and insertion of cations: acting the material as a cation exchanger.

Scheme 2. a) Electropolymerization process of EDOT to produce PEDOT. b) Polymer reduction reaction for PEDOT.

Scheme 3. a) Polymers with *o*- and *m*-carborane linked by C_c; b) polymers with *o*-carboranyl linked by the B_c.

Scheme 4. Synthesis of benzocarborane fused polymers **35**.

Scheme 5. Synthesis of polymer **37.**

Scheme 6. Synthesis of polymer type **38** using $B_{10}H_{14}$**.**

Scheme 7. Microwave assisted preparation of polymers **40** and **41** at 200 ºC for 30 min. in the presence of $[Pd_2(dba)_3]$ and P(*o*-tol)$_3$ in chlorobenzene.

Scheme 8. Synthesis of polymers **43**, **45a** and **45b**.

Scheme 9. Microwave-assisted homopolymerization and copolymerization of monomer **46** to produce polymers **47** and **48**, respectively.

Scheme 10. Preparation of the polynorbornene copolymers **49** and **50.**

Scheme 11. Preparation of poly-aryl(ether-ketone)s containing *m*-carborane**.**

Scheme 12. Preparation of polyimides bearing the *m*-carborane cluster.

Scheme 13. Synthesis of polymer **55** by "click" reaction.

Scheme 14. Preparation and dendronization of polymer **56**.

Scheme 15. Formation of carborane-containing diblock copolymers.

Scheme 16. Preparation of carborane-siloxane-acetylene polymers.

Scheme 17. Example of the preparation of *m*-carborane-siloxane polymers via Karstedt-catalyzed hydrosilyation reaction.

Scheme 18. Preparation of poly(carborane-siloxane arylacetylene) polymers **62** and **63.**

Scheme 19. Preparation of polymer **64**.

Scheme 20. Preparation of poly(siloxane-arylacetylene)s **65** from $B_{10}H_{14}$.

Scheme 21. Procedure for the preparation of poly(carboranesilanec) **66**.

Scheme 22. Preparation of polymers **67** and **68**.

Scheme 1. The oxidation-reduction process in PPy(**1**) occurs via de-insertion and insertion of cations: acting the material as a cation exchanger.

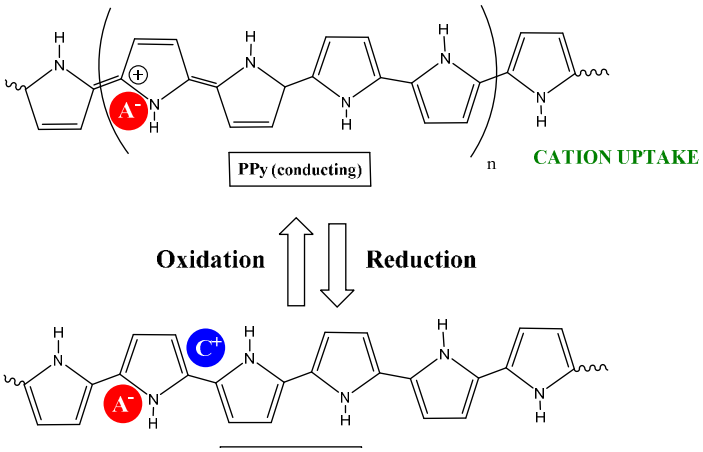

Scheme 2. a) Electropolymerization process of EDOT to produce PEDOT. b) Polymer reduction reaction for PEDOT.

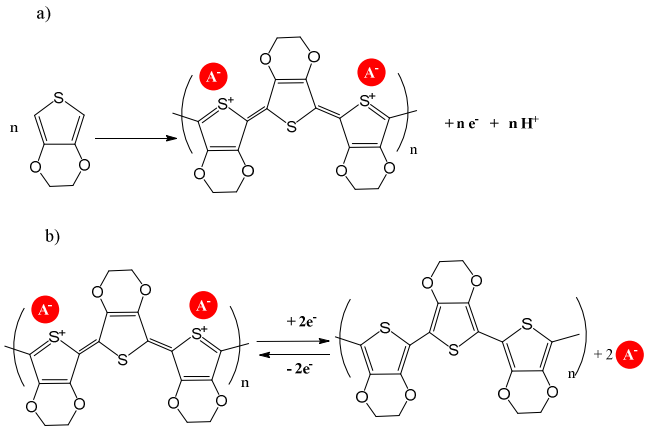

Scheme 3. a) Polymers with *o*- and *m*-carborane linked by C_c; b) polymers with *o*-carboranyl linked by the B_c.

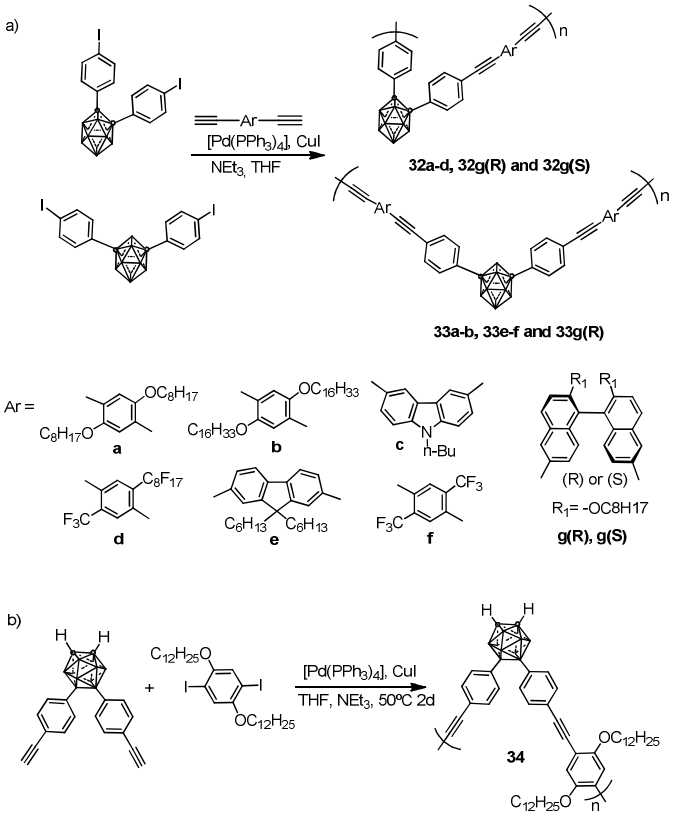

Scheme 4. Synthesis of benzocarborane fused polymers **35**.

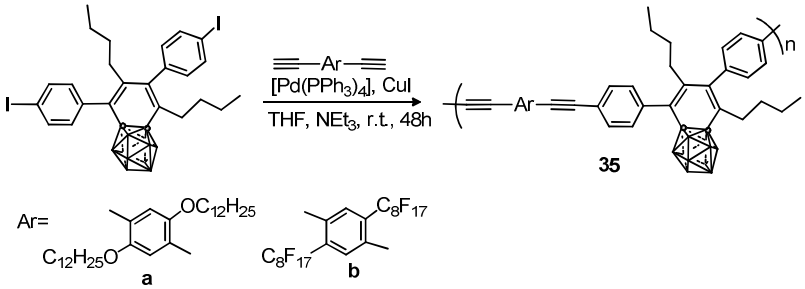

Scheme 5. Synthesis of polymer **37.**

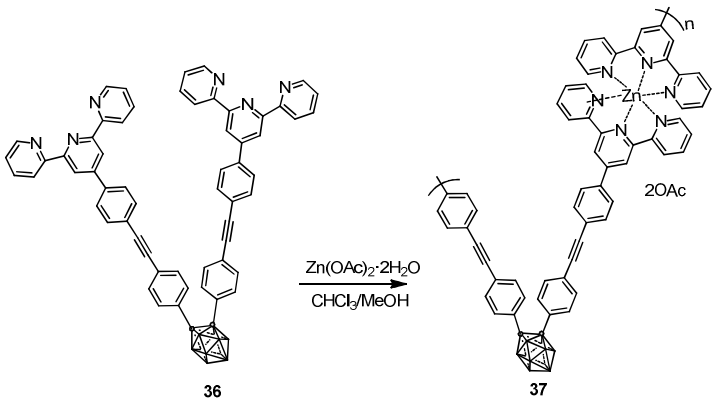

Scheme 6. Synthesis of polymer type **38** using $B_{10}H_{14}$**.**

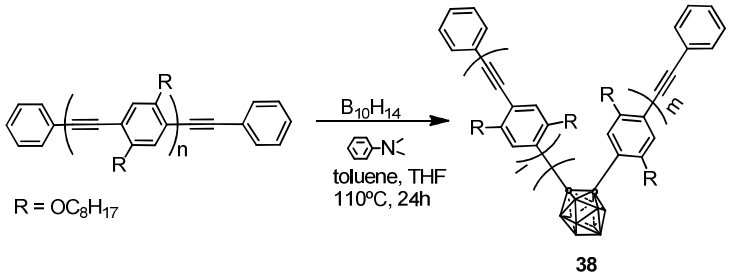

Scheme 7. Microwave assisted preparation of polymers **40** and **41** at 200 ºC for 30 min. in the presence of $[Pd_2(dba)_3]$ and P(*o*-tol)$_3$ in chlorobenzene.

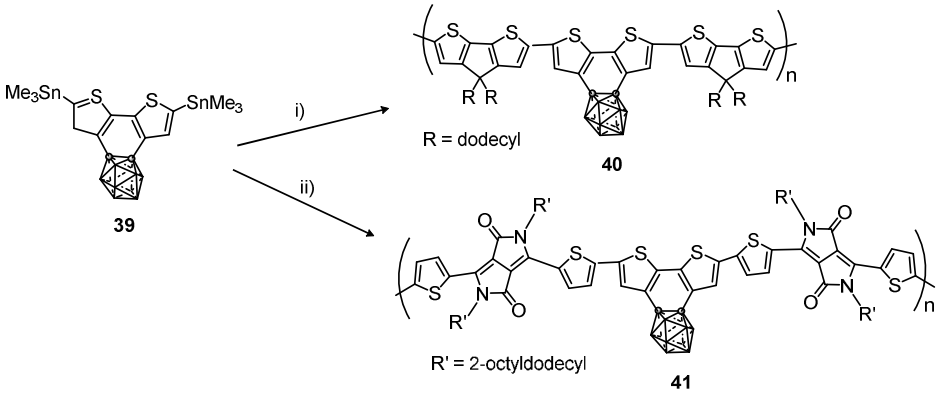

i) 2,6-dibromo-4,4-bis(dodecyl)-4H-cyclopenta[2,1-b;3,4-b']dithiophene
ii) 3,6-bis(2-bromothien-5-yl)2,5-bis(2-octyldodecyl)pyrolo[2,4-c]pyrole-1,4(2H,5H)-dione

Scheme 8. Synthesis of polymers **43**, **45a** and **45b**.

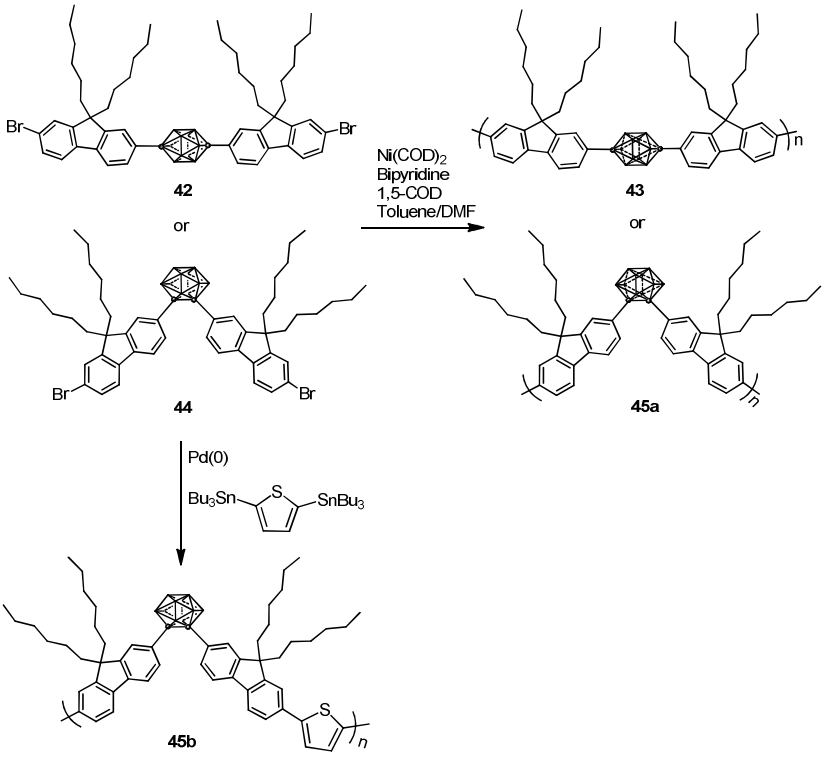

Scheme 9. Microwave-assisted homopolymerization and copolymerization of monomer **46** to produce polymers **47** and **48**, respectively.

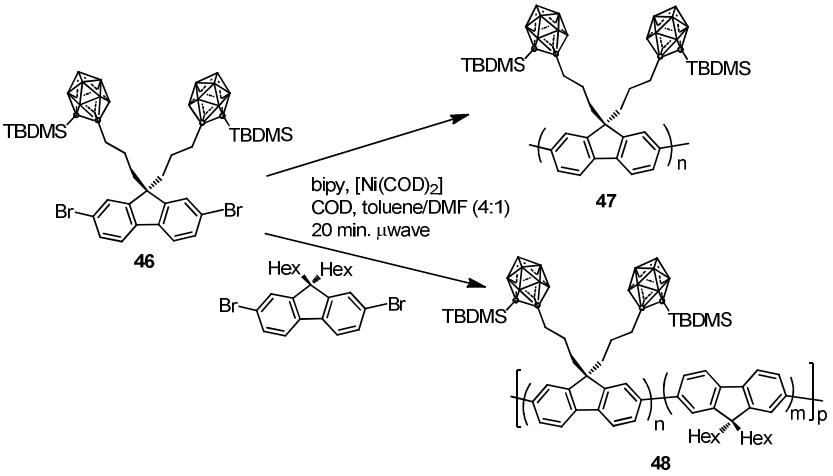

Scheme 10. Preparation of the polynorbornene copolymers **49** and **50.**

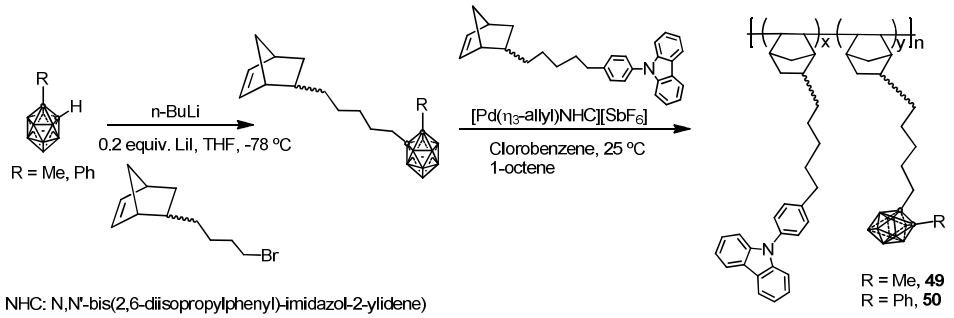

Scheme 11. Preparation of poly-aryl(ether-ketone)s containing *m*-carborane**.**

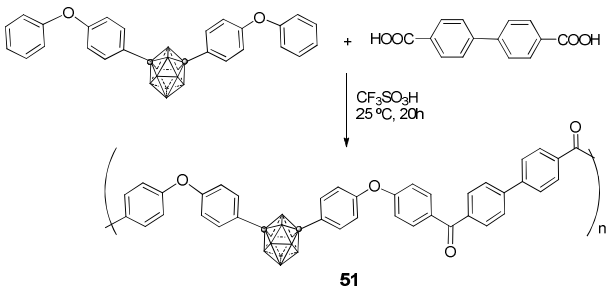

51

Scheme 12. Preparation of polyimides bearing the *m*-carborane cluster.

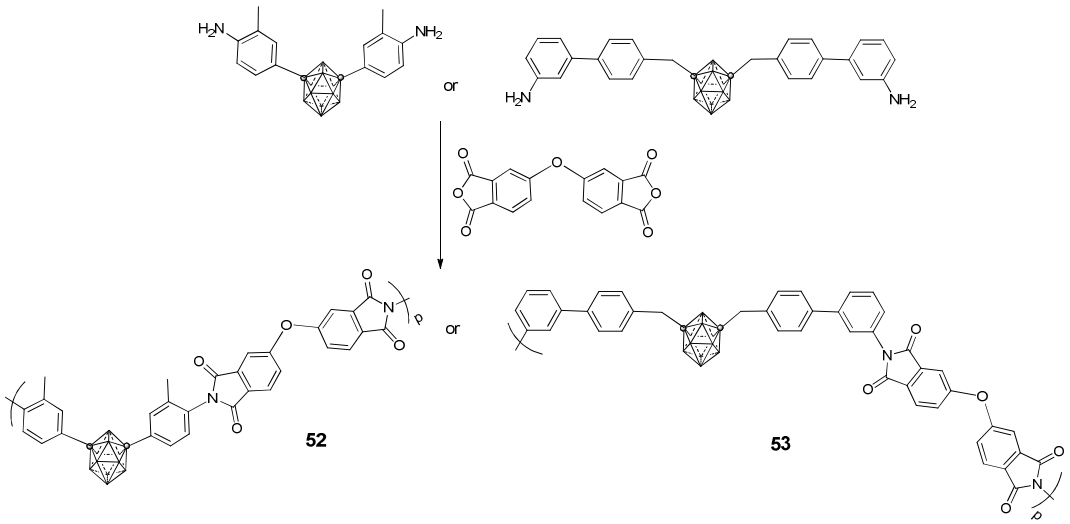

Scheme 13. Synthesis of polymer **55** by "click" reaction.

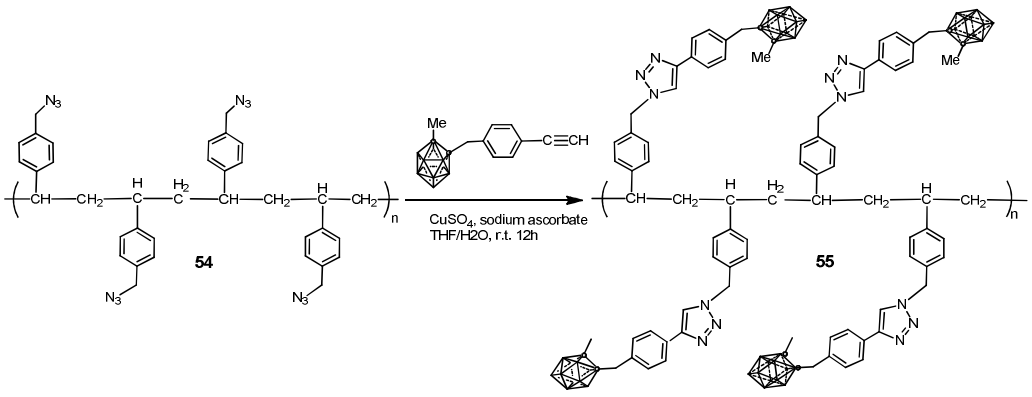

Scheme 14. Preparation and dendronization of polymer **56**.

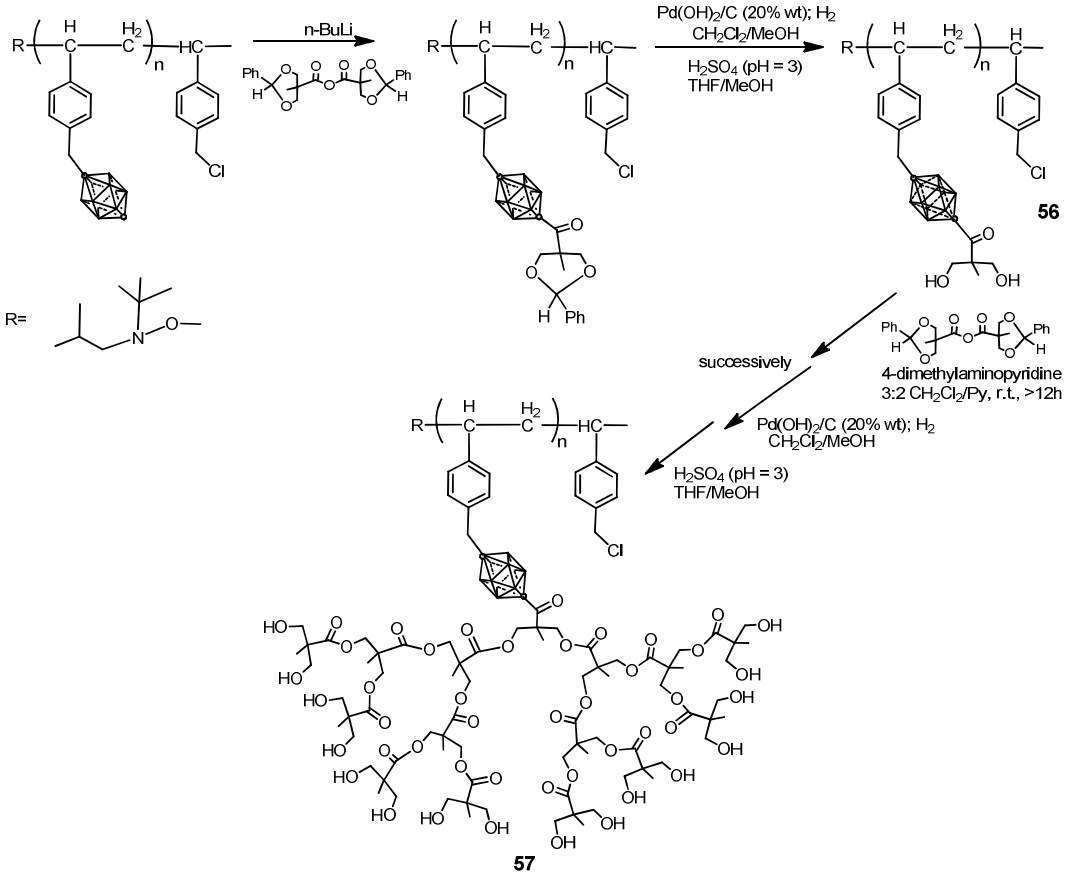

Scheme 15. Formation of carborane-containing diblock copolymers.

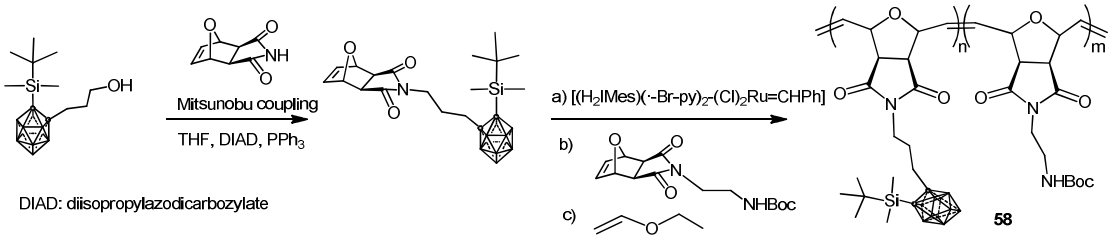

Scheme 16. Preparation of carborane-siloxane-acetylene polymers.

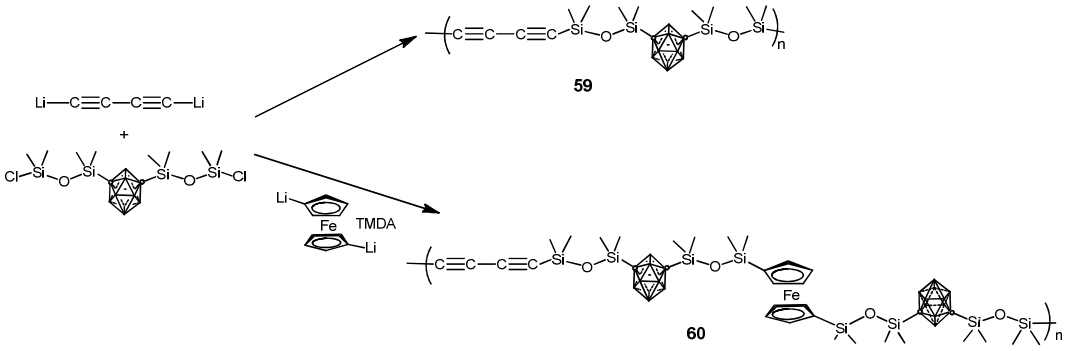

Scheme 17. Example of the preparation of *m*-carborane-siloxane polymers via Karstedt-catalyzed hydrosilyation reaction.

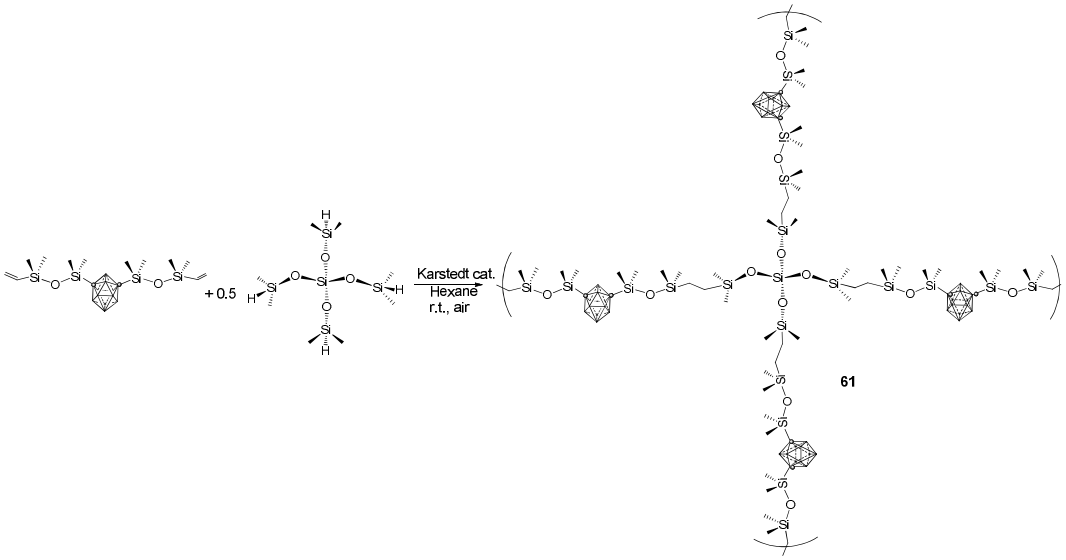

Scheme 18. Preparation of poly(carborane-siloxane arylacetylene) polymers **62** and **63.**

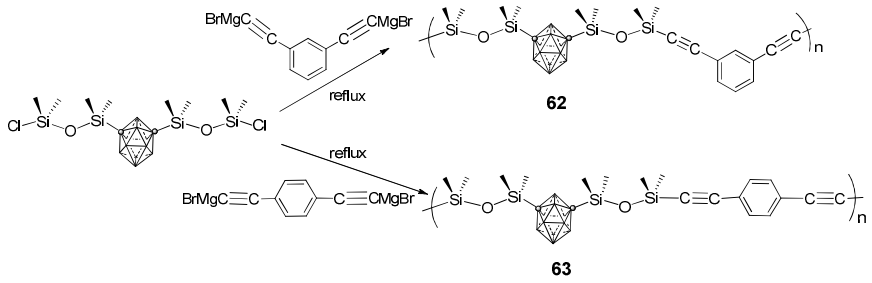

Scheme 19. Preparation of polymer **64**.

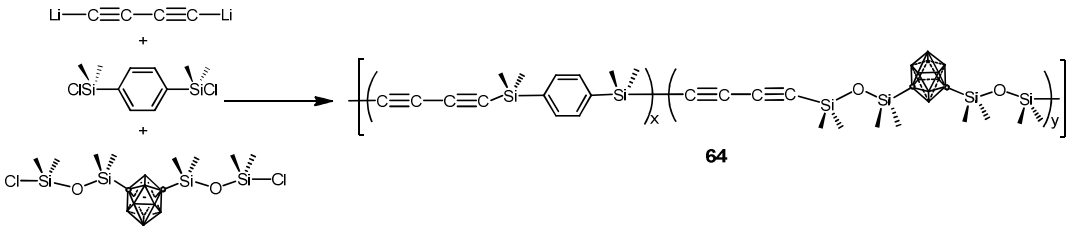

Scheme 20. Preparation of poly(siloxane-arylacetylene)s **65** from $B_{10}H_{14}$.

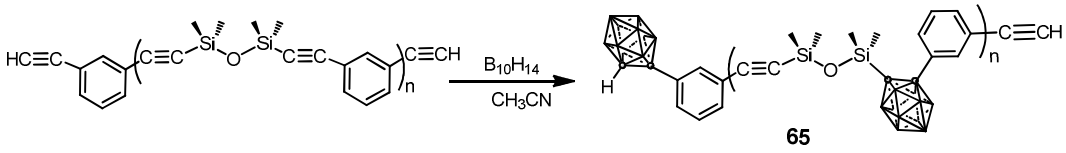

Scheme 21. Procedure for the preparation of poly(carboranesilanec) **66**.

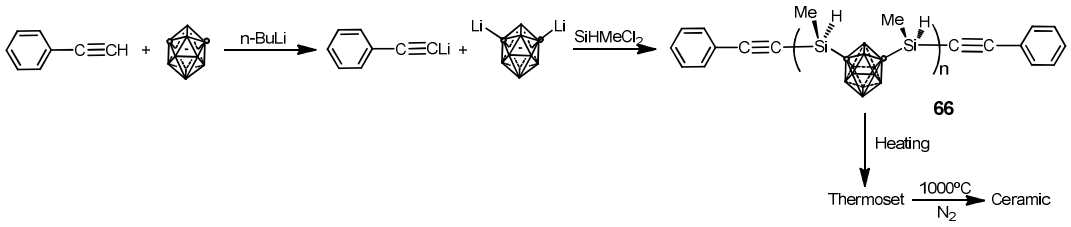

Scheme 22. Preparation of polymers **67** and **68**.

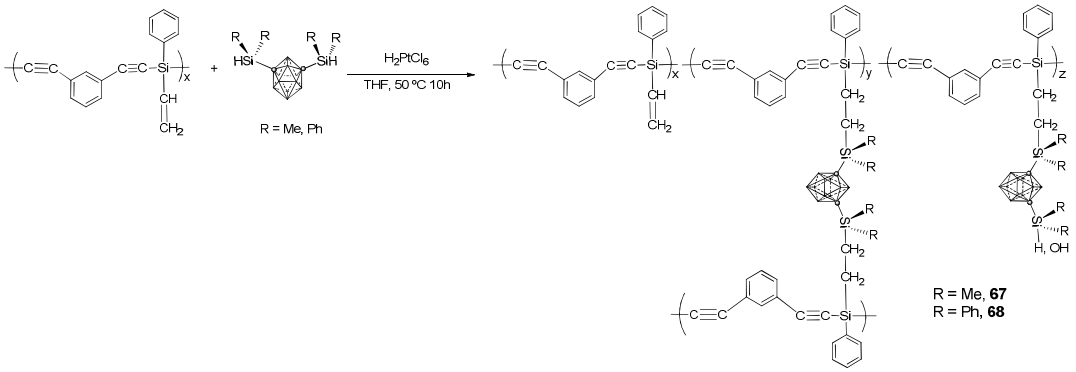

TABLES CAPTION

Table 1. ORL values (in Volts) of different PPy films doped with anionic icosahedral shape boron clusters, PPy(**1**)-PPy(**17**); PPy films containing icosahedral boron clusters doped with $[\mathbf{PF_6}]^-$ compared with PPy polymers doped with common anions.

Table 2. Photophysical properties of polymers.

Table 1. ORL values (in Volts) of different PPy films doped with anionic icosahedral shape boron clusters, PPy(**1**)-PPy(**17**); PPy films containing icosahedral boron clusters doped with $[\mathbf{PF_6}]^-$ compared with PPy polymers doped with common anions.

Compound	ORL (in Volts)	Compound	ORL (in Volts)
PPy(**1**)	1.257	PPy(**12**)	1.33[10]
PPy(**3**)	0.91[10]	PPy(**12**)	1.33[10]
PPy(**4**)	0.96[10]	PPy(**13**)	1.41[10]
PPy(**5**)	0.99[10]	PPy(**14**)	1.45[10]
PPy(**6**)	1.15[10]	PPy(**17**) copolymer	No observation of a defined peak in the range 0-1.8 V5
PPy(**7**)	0.90[10]	PPy($\mathbf{PF_6}$)	0.897
PPy(**9**)	1.21[10]	PPy(**DBS**)	0.937
PPy(**10**)	1.15[10]	PPy($\mathbf{ClO_4}$)	0.95
PPy(**11**)	1.27[10]		

Table 2. Photophysical properties of polymers.

Compound	Compound CB Isomer	Solvent	λ_{abs} (nm)	λ_{em} (nm)	ϕ_F
32a	*ortho*	THF	379	559[a]	3.8[a]
32b	*ortho*	THF	380	550[a]	n.d
32c	*ortho*	THF	358	583[a]	n.d
32d	*ortho*	THF	345	405	n.d
33a	*meta*	$CHCl_3$	314,378	415	0.25
33b	*meta*	$CHCl_3$	314,378	415	0.25
33e	*meta*	$CHCl_3$	319,362	386,410	0.11
33f	*meta*	$CHCl_3$	345,366	409	0.22
32g(R)	*ortho*	THF	241, 283, 338	566[a] (562)[b]	0.05[a] (0.23)[b]
33g(R)	*meta*	THF	239, 292, 335	388 (562)[b]	0.50 (0.09)[b]
34	*ortho*	$CHCl_3$	413[b]	403	0.38
35a	*ortho*	THF	312,375	411,430	0.51
35b	*ortho*	THF	353,368	383,410	0.40
36	*ortho*	$CHCl_3$–CH_3OH	314	440	<0.002
37	*ortho*	$CHCl_3$–CH_3OH	334	465	0.18
38	*ortho*	THF	428	471 (529)[a]	n.d
40	*ortho*	chlorobencene	550 (543)[b]	n.d.	n.d.
41	*ortho*	chlorobencene	784 (793)[b]	n.d.	n.d.
43	*para*	$CHCl_3$	n.d.	400	n.d.
45a	*ortho*	$CHCl_3$	384[c]	423 (563)[b] (565)[c]	n.d.
45b	*ortho*	$CHCl_3$	441[c]	602 (570)[b]	n.d
47	*ortho*	-	n.d.	535[d]	n.d
48	*ortho*	-	n.d	535[ed]	n.d
49	*Ph-ortho*		292,330,341	-	
50	*Me-ortho*		292,330,341	351,366	

[a]Measured in THF/H_2O (1/99) (v/v) at room temperature. [b] Thin film. [c]$\lambda_{max,edge}$. [d]Thin films before and after annealing 3h at 200 ºC

[1] H. Shirakawa, E. J. Louis, A. G. MacDiarmid, Ch. K. Chiang, A. J. Heeger, *J. Chem. Soc., Chem. Commun.*, 1977, **16**, 578-580.

[2] R. McNeill, R. Siudak, J.H. Wardlaw and D.E. Weiss, *Aust. J. Chem*., 1963, **16**, 1056-1075 and references therein.

[3] A. F. Diaz, K. K. Kanazawa, and G. P. Gardini, *J. Chem. Soc., Chem. Commun*., 1979, 635-636.

[4] R.N. Grimes "Carboranes" 2nd Edition, Academic Press: Burlington, MA, **2011**.

[5] C. Masalles, J. Llop, C. Viñas and F. Teixidor, *Adv. Mater*., 2002, **14**, 826-829.

[6] V. Savvateev, A. Yakimov and D. Davidov, *Adv. Mater.*, 1999, **11**, 519-585.

[7] C. Masalles, S. Borrós, C. Viñas and F. Teixidor*, Adv. Mater*., 2000, **12**, 1199-1202.

[8] C. Masalles, S. Borrós, C. Viñas and F. Teixidor, *Adv. Mater*., 2002, **14**, 449-452.

[9] C. Viñas, M. Tarrés, P. González-Cardoso, P. Farràs, P. Bauduin and F. Teixidor, *Dalton Trans.,* 2014, **43**, 5062-5068.

[10] S. Gentil, E. Crespo, I. Rojo, A. Friang, C. Viñas, F. Teixidor, B. Grüner and D. Gabel, *Polymer*, 2005, **46**, 12218-12225.

[11] J. Llop, C. Masalles, C. Viñas, F. Teixidor, R. Sillanpää and R. Kivekäs, *Dalton Trans.,* **2003**, 556-561.

[12] E. Crespo, S. Gentil, C. Viñas and F. Teixidor, *J. Phys. Chem. C*, 2007, **111**, 18381-18386.

[13] J. Mola, E. Mas-Marza, X. Sala, I. Romero, M. Rodríguez, C. Viñas, T. Parella and A. Llobet, *Angew. Chem. Int. Ed.*, 2008, **47**, 5830-5832.

[14] B. Fabre, J. Caleb Clark and M. G. Vicente, *Macromolecules*, 2006, **39**, 112-119.

[15] E. Hao, B. Fabre, F. R. Fronczek and M. G. Vicente, *Chem. Mater.*, 2007, **19**, 6195-6105.

[16] S. Chayer, L. Jaquinod, K. M. Smith and M. G. Vicente, *Tetrahedron Lett*., 2001, **42**, 7759-7761.

[17] B. Fabre, S. Chayer and M. G. Vicente, *Electrochemistry Commun.*, 2003, **5**, 431-434.

[18] E. Hao, B. Fabre, F.R. Fronczek and M.G.H. Vicente, *Chem. Commun*., 2007, 4387-4389.

[19] F. Barriere, B. Fabre, E. Hao, Z.M. LeJeune, E. Hwang, J.C. Garno, E. Nesterov and M.G.H. Vicente, *Macromolecules*, 2009, **42**, 2981-2987.

[20] V. David, C. Viñas, F. Teixidor, *Polymer*, 2006, **47**, 4694-4702.

[21] E.M. Cansu-Ergun and A. Cihaner, *J. Electroanal. Chem*., 2013, **707**, 78-84.

[22] M. Asay, C.E. Kefalidis, J.Estrada, D.S. Weinberger, J. Wright, C. Moore, A. L. Rheingold, L. Maron, V. Lavallo, *Angew. Chem. Int. Ed,* 2013, **52**, 11560-11563.

[23] J. H. Wright, II, C.E. Kefaidis, F.S. Tham, L. Maron and V. Lavallo, *Inorg. Chem*., 2013, **52**, 6223-6229.

[24] M. Tominaga, Y. Morisaki and Y. Chujo *Macromol. Rapid Commun.* 2013*,* **34***,* 1357−1362, and references therein.

[25] K. Kokado, M. Tominaga and Y. Chujo, *Macromol. Rapid Commun.* 2010, **31**, 1389–1394.

[26] K. Kokado and Y. Chujo, *Dalton Trans*., 2011, **40**, 1919-1923.

[27] K. Kokado and Y. Chujo, *Polym. J*., 2010, **42**, 363–367.

[28] J Marshall, B. C. Schroeder, H. Bronstein, I. Meager, S. Rossbauer, N. Yaacobi-Gross, E. Buchaca-Domingo, T. D. Anthopoulos, N. Stingelin, P. Beavis and Martin Heeney, *Macromolecules* 2014, **47**, 89−96.

[29] J. J. Peterson, M. Werre, Y. C. Simon, E. B. Coughlin and K. R. Carter, *Macromolecules* 2009, **42**, 8594–8598.

[30] A. R. Davis, J. J. Peterson and K. R. Carter, *ACS Macro Lett*. 2012, **1**, 469−472.

[31] Y. C. Simon, J. J. Peterson, C. Mangold, Kenneth R. Carter and E. B. Coughlin, *Macromolecules,* 2009, **42**, 512-516.

[32] K. C. Eo, M. H. Park, T. Kim, Y. Do and M. H. Lee, *Polymer*, 2013, 6321-6328.

[33] a) H. M. Colquhoun, D. F. Lewis, J. A. Daniels, P. L. Herbertson, J. A. H. MacBride, R. Stephenson and K. Wade, *Polymer*, 1997, 2447-2453, and references therein.

[34] Xing, T.; Zhang K., *Polym. Int*., 2015; **64**, 1715–1721.

[35] L. Liang, A. Rapakousiou, L. Salmon, J. Ruiz, D. Astruc, B. P. Dash, R. Satapathy, J. W. Sawicki and N. S. Hosmane, *Eur. J. Inorg. Chem.,* 2011, 3043–3049.

[36] S. R. Benhabbour, M. C. Parrott, S. E. A; Gratton and A. Adronov, *Macromolecules,* 2007, *40*, 5678-5688.

[37] Y. C. Simon, C. Ohm, M. J. Zimny and E. Bryan Coughlin, *Macromolecules,* 2007, **40**, 5628-5630.

[38] M. K. Kolel-Veetil, H. W. Beckham and T. M. Keller, *Chem. Mater.,* 2004, **16***,* 3162-3167, and references therein.

[39] M. K. Kolel-Veetil and T. M. Keller, *J. Polym. Sci. Part A: Polym. Chem*., 2006, **44**, 147–155.

[40] M. K. Kolel-Veetil, D. D. Dominguez, C. A. Klug, K. P. Fears, S. B. Qadri, D. Fragiadakis and T. M. Keller, *J. Polym. Sci. Part A: Polm. Chem*., 2013, **51**, 2638–2650.

[41] Y. Jiang, X. Li, F. Huang, Y. Zhou and L. Du, J. *Macromol. Sci., Part A: Pure Appl. Chem*., 2015, **52**, 476–484, and references therein.

[42] H. Kimura,| K. Okita, M. Ichitani, T. Sugimoto, S. Kurok and I. Ando, *Chem. Mater.,* 2003, **15***,* 355-362, and references therein.

[43] C. E. Housecroft, *J. Organomet. Chem.,* 2015, **798**, 218-228.

[44] G. Zi, H-W. Li and Z. Xie, *Organometallics,* 2002, **21**, 5415-5427.

[45] L. Deng, M-S. Cheung, H-S. Chan and Z. Xie, *Organometallics* 2005, **24**, 6244-6249.

[46] K. Chui, H-W. Li and Z. Xie, *Organometallics,* 2000, **19**, 5447-5453.

[47] J. H. Wrigh, G. W. Mueck, F. S. Tham and C. A. Reed, *Organometallics,* 2010, **29**, 4066-4070.

[48] I. Rojo, F. Teixidor, C. Viñas, R. Kivekäs, and R. Sillanpää, *Chem. Eur. J.,* 2004, **10**, 5376-5387.

[49] M. Fontanet, M. Rodríguez, I. Romero, X. Fontrodona, F. Teixidor, C. Viñas, N. Aliaga-Alcalde and P. Matějíček, *Dalton Trans*., 2014, **42**, 7838-7841.

[50] M. Fontanet, M. Rodríguez, X. Fontrodona, I. Romero, F. Teixidor, C. Viñas, N. Aliaga-Alcalde and P. Matějíček, *Chem. Eur. J.*, 2014, **20**, 13993-14003.

[51] S. Wang, H-W. Li and Z. Xie, *Organometallics,* 2004, **23**, 2469-2478.

[52] R. Khattar, M.J. Manning, C.B. Knobler, S.E. Johnson and M.F. Hawthorne*, Inorg. Chem*., 1992, **31**, 268-273.

[53] S. Wang, Y. Wang, M-S. Cheung, H-S. Chan and Z. Xie, *Tetrahedron,* 2003, **59**, 10373-10380.

[54] K. Chui, Q. Yang, T.C.W. Mak and Z. Xie, *Organometallics*, 2000, **19**, 1391-1401 and references therein.

[55] M-S. Cheung, H-S. Chan and Z. Xie, *Organometallics,* 2005, **24**, 4468-4474.